Bivariate Population Balance Model of Ethanol-Fueled Spray Combustors

Daniel E. Rosner
High Temperature Chemical Reaction Engineering Laboratory and Yale Center for Combustion Studies, Dept. of Chemical and Environmental Engineering, Yale University, New Haven, CT 06520

Manuel Arias-Zugasti
Departamento de Física Matemática y de Fluidos, Facultad de Ciencias UNED, Apdo: 60141, 28080 Madrid, Spain

DOI 10.1002/aic.12552
Published online March 31, 2011 in Wiley Online Library (wileyonlinelibrary.com).

We present a bivariate population balance-based formulation of the performance of well-mixed adiabatic combustors fed by ethanol (EtOH)-containing sprays of prescribed droplet size distribution (DSD) and composition. Our historically interesting example is the fuel-cooled V-2 chemical rocket—using 75 wt % EtOH + H_2O solution, and oxidizer O_2(L). Of special interest are the predicted combustion "intensity" (GW/m^3) and efficiency (EtOH fraction vaporized) at each ratio of combustor mean residence time to feed-droplet characteristic vaporization time. Our formulation exploits a quasi-steady, gas-diffusion-controlled individual droplet evaporation rate law, and the method-of-characteristics to solve the associated first-order population balance partial differential equation governing the joint distribution function $n(m_1, m_2)$ of the fuel spray exiting such a chamber, where m_1 = EtOH mass/droplet, and m_2 = H_2O mass/droplet. Besides the combustor efficiency and intensity, this bivariate distribution function enables predictions of corresponding unconditional DSD, and the joint distribution function(diam., droplet temperature)—perhaps measurable. Our numerically exact formulation/results also provide valuable test cases for convenient approximate methods (bivariate moment and spectral/weighted residual) to predict these "correlated" bivariate distribution functions in more complex situations. © 2011 American Institute of Chemical Engineers *AIChE J*, 57: 3534–3554, 2011
Keywords: bivariate population balance, ethanol-fueled spray combustors, liquid biofuel performance, liquid propellant chemical rockets, evaporation-controlled combustion intensity, multiphase chemical reaction engineering

Introduction: Background, Motivation, and Objectives

Spray-fuel fed steady-flow combustors can profitably be investigated by adopting a population-balance viewpoint (e.g., Ref. 1)—coupling the evaporating fuel spray population with the surrounding gas mixture (assuming the oxidizer is gaseous, e.g., O_2-enriched, or, perhaps, "vitiated" air). In Ref. 1, we treated the limiting case of a well-macromixed adiabatic combustor containing single-component (kerosene-like) droplets but allowed for the intrinsically transient nature of the gas-diffusion-controlled droplet vaporization process—especially important for high-pressure (above ca. 10 atm for such hydrocarbons) operation. We demonstrated that the performance of such device could be calculated in terms of the univariate fuel droplet number density distribution function: (NDDF)

Preliminary versions of portions of this article were presented at AIChE 2008 Annual Meeting (Philadelphia) Paper #156d, and AIChE 2010 Annual Meeting (Salt Lake City) Paper #694a.
Correspondence concerning this article should be addressed to D. E. Rosner at daniel.rosner@yale.edu.

$n(v)$—in terms of which the combustor efficiency and "intensity" (chemical heat release rate per unit volume) could be readily calculated via quadratures. In this present extension of Ref. 1, we now formulate/present the results of a bivariate population balance (PB)-based theoretical analysis of the performance of well-(macro-)mixed adiabatic combustors fed by ethanol (EtOH)- containing sprays of prescribed droplet size distribution (DSD) and composition. One of our goals is to anticipate some features to be expected when using a prominent "bio-fuel" like EtOH—which has the intriguing property of absorbing its own combustion product (H_2O)! However, our "pre-bio-fuel" historically relevant/instructive numerical example will be the rather well-documented liquid fuel-cooled V-2 chemical rocket—which actually used 75 wt % EtOH + H_2O solution as its "fuel," along with the cryogenic oxidizer O_2(L) at a chamber pressure of 15 atm. Of special interest are our predicted combustion intensities (chemical energy release rate, GW/m^3), and efficiencies (related to EtOH fraction vaporized) at each "vaporization Damköhler number" (i.e., ratio of combustor vapor mean residence time to feed Sauter-mean-diameter-(d_{32})-based quasi-steady (QS)-droplet vaporization lifetime). Our present formulation exploits a QS gas-diffusion-controlled and internally well-mixed individual droplet evaporation rate law, and we exploit the formally exact method-of-characteristics to solve the associated first-order population-balance partial differential equation (PDE) governing the joint NDDF exiting such a chamber. We demonstrate that this NDDF also enables predictions of corresponding unconditional DSD as well as the possibly (remotely-) measurable joint distribution function in terms of droplet diameter and droplet temperature. Apart from their intrinsic multiphase chemical reaction-engineering interest, as an instructive, tractable limiting case, our numerically exact formulation/results can now also provide valuable "meter-sticks" for computationally convenient approximate population balanced equation (PBE) solution methods (e.g., bivariate quadrature method of moments (QMOM) and spectral/weighted residuals) to predict such "correlated" NDDFs in more realistic/complex spray combustor environments. We will also be able to demonstrate the inability of a seemingly plausible "pseudo-unary" approximation to capture key features of the combustion intensity achievable in such alcohol-fueled combustors. Lastly, generalizations of possible future interest to chemical reaction engineers will be outlined.

It should be recognized that such spray fuel fed combustors are now common to many strategic technologies, spanning commodity chemical synthesis, power generation, and chemical propulsion (both aircraft- and rocket-based). Although many important design-constraints obviously differ from application-to-application, such combustors share certain common performance characteristics, and the high cost of conceiving/developing/testing new devices certainly provides powerful economic incentives to develop rational yet tractable design methods for them. Of course, the variety and complexity of spray combustors, together with the sparsity of well-characterized/documented performance data, continues to pose formidable challenges to analysts and designers. A broad spectrum of mathematical/numerical tools and models is, in fact, needed to provide timely information about how the device performance will depend on such factors as: geometry, inlet conditions (both liquid phase and gas phase), liquid fuel properties, and injector ("atomizer") performance. Such information can, of course, not only be used for purposes of engineering design but also to anticipate the consequences of, say, fuel substitution, oxygen enrichment (nitrogen reduction), introduction of fuel blends or additives, and even to guide the model-based control strategies.

This work is motivated, in part, by the belief that rational yet tractable computational models will require more than advances in computer science/technology. Because of the wide range of operative (length and time) scales encountered in this class of multiphase chemically reacting flow problems, in the foreseeable future clever approximations, often based on rational asymptotic methods applied to simpler "model problems," will continue to be required to capture the essential physicochemical phenomena while keeping the associated numerical simulations manageable.

This work, offered in this spirit, will hopefully play a role in cutting the currently high cost and lead times for new spray combustor R&D. Specifically, for this present paper, our goals include providing: (1) A tractable, population-balance based mathematical model to economically guide the development of more comprehensive models of continuous spray combustor performance; (2) "Metersticks" for the testing/evaluation of rival mathematical/numerical methods (QMOM, Monte-Carlo,…) to solve such multivariate population-balance problems; (3) an instructive extension of our previous "univariate" analysis (Ref. 1) of pure fuel (unary-) spray combustor performance; (4) insight into the behavior of an important "biofuel" (here EtOH) which is a solvent for its own combustion product (H_2O); (5) a basis for needed extensions to embrace more complex fuel blends, intra-droplet diffusional resistance, inclusion of chemical kinetic limitations on efficiency, predictions of pollutant production, etc.

The following account of our present theoretical approach, illustrative results, and discussion is structured as follows: The idealizations and basic assumptions underlying our mathematical model are first set forth in the "Mathematical Model: Idealized Ethanol-Fueled Spray Combustor" Section, which includes a summary of our QS treatment of individual binary droplet vaporization as well as the PBE that couples the spray vaporization dynamics to the current ambient conditions in the combustion chamber. In this section, we also explain the basic property data considered in the numerical calculations. Our formally exact Eulerian characteristics-based bivariate population balance method for dealing with the evolution of a prescribed injected 2-component (EtOH + H_2O) spray is presented in the "Theoretical Development: Choice of Mathematical and Numerical Methods" Section. Our iterative method for coupling the vaporizing binary fuel spray with the "surrounding," combusting gas phase is shown in the "Coupling Between the Dispersed (Fuel Spray) and Continuous Phases; Self-Consistent Steady-State Chamber Composition and Temperature" Section. Here, we also identify/outline the computation of two dimensionless performance indices of special importance, viz. the loss in efficiency associated with the fraction, $f_{1,\mathrm{unevap}}$, of the original EtOH-containing* liquid spray

*Although we select ethanol for our present illustrative numerical results, the present analysis will clearly carry over without change to the alternative bio-fuel methanol (=CH_3OH)i.e., only the values of our key parameters (f_{stoich}, Q_{comb}, L_{vap},…) need be modified, not our procedures.

which remains unevaporated in the available mean chamber residence time, and the volumetric chemical energy release rate (i.e., combustion "intensity") associated with steady, adiabatic operation. This provides the basis for the theoretical/computational developments outlined in the "Theoretical Development: Choice of Mathematical and Numerical Methods" Section, which describes our "exact" numerical solution strategy. Our numerical illustrations and several parametric studies are collected in the "Illustrative Quantitative Results: Von Braun's V-2 Liquid Propellant Rocket Motor" Section, emphasizing results for the historically important special case of the EtOH-fueled German V-2 liquid propellant rocket motor of World War II. Following a critical discussion of these new results, we refocus on our principal new underlying assumptions in our "Discussion: Defense of Assumptions, Implications of Results, and Applications" Section, defending some and delimiting the validity of others. Immediate and/or less-obvious implications and extensions are also indicated there. The Conclusions and Broader Engineering Implications Section, which completes this article, summarizes our principal conclusions and recommendations, re-emphasizing the potential value of this class of theoretical models for the preliminary testing of conjectured simplifications. For a more in-depth discussion of complementary spray-combustor performance models that have been developed in the last 100 years, the reader is directed to Ref. 2.

Mathematical Model: Idealized Ethanol-Fueled Spray Combustor

Underlying assumptions

In this model, we assume that the spray droplets are internally well-mixed, i.e., droplet composition as well as droplet temperature, depend only on time, but not on radial position within each droplet. Later, when we solve the PBE that determines the evolution of the spray, we will also assume that all the droplets in the spray are at their respective "wet-bulb" temperatures (T_{WB}), which, as shown below, depends only on droplet composition, but is independent of droplet size. As a consequence, the population of spray fuel droplets is considered bivariate, which can be described either by the amount of EtOH m_1 and water m_2 in each droplet, or by any other choice of equivalent variables, such as total mass $m = m_1 + m_2$ and droplet composition (e.g., in terms of EtOH mass fraction ω).

As shown below, the assumption that each droplet in the spray is at the corresponding composition-dependent (and time dependent) T_{WB} relies on two further assumptions: the initial spray temperature is close to T_{WB} corresponding to the initial spray composition and the droplet temperature remains at the time-dependent T_{WB} as its composition changes (because EtOH vaporizes faster than water). The first assumption was explicitly examined in Rosner et al.[1] The second assumption has been justified using illustrative calculations of time evolution of individual droplets under prescribed ambient conditions, where it is shown that the temperature adjusts almost instantaneously to the time dependent T_{WB}.

On the other hand, the combustion chamber will be considered well-macro-mixed, described by overall, time-independent values of the time- and volume-averaged temperature, and composition. Of course, this forfeits potentially useful spatial information—for which higher dimensional models are needed.[3,2]

Quasi-steady diffusion-controlled rate laws governing $\dot{m}_1$ and $\dot{m}_2$

Rate laws that govern the time evolution of EtOH (subscript 1) and water (subscript 2) mass (m_1 and m_2), and energy, for each individual droplet, are required. In this model, we consider the droplets to be internally well-mixed. As a consequence, the evolution rate laws are dictated by the mass and energy balances at the droplet radius (R)—i.e., at the L/V interface between the liquid droplet and its surrounding atmosphere. The QS rate laws adopted for m_1 and m_2 are given by the following expressions

$$\frac{dm_1}{dt} = -4\pi R^2 \cdot \left(Pe_m \, \rho_{ref} D_{ref} \, \frac{\omega_{1,w}}{R} + F(Pe_m) \, \rho_f D_{1,f} \, \frac{\omega_{1,w} - \omega_{1,e}}{R} \right) \quad (1)$$

$$\frac{dm_2}{dt} = -4\pi R^2 \cdot \left(Pe_m \, \rho_{ref} D_{ref} \, \frac{\omega_{2,w}}{R} + F(Pe_m) \, \rho_f D_{2,f} \, \frac{\omega_{2,w} - \omega_{2,e}}{R} \right) \quad (2)$$

Here Pe_m is a mass-transfer Peclet number, defined by $Pe_m \equiv v_w d_w / D$, which can be shown to be related to the mass driving force (B_m) by:

$$Pe_m = \ln(1 + B_m), \quad F(Pe_m) = \frac{\ln(1 + B_m)}{B_m} \quad (3)$$

with

$$B_m = \frac{\frac{D_{1,f}}{D_{ref}} (\omega_{1,w} - \omega_{1,e}) + \frac{D_{2,f}}{D_{ref}} (\omega_{2,w} - \omega_{2,e})}{1 - \omega_{1,w} - \omega_{2,w}} \quad (4)$$

Note that, in the limit that species 1 and 2 become indistinguishable, these equations reduce (as they must) to the familiar QS-evaporation rate equations for a single component droplet (see, e.g., Ref. 4).

In the former expressions, ρ is the gas mass density, ω_i the mass fraction of species i, subscripts w and e refer to the droplet surface and exterior (far-field) gas conditions, respectively, whereas subscript f refers to evaluation at average "film" conditions in the gas (determined here according to the familiar 2/3 rule: $X_f = (2/3)\, X_w + (1/3)\, X_e$—for any quantity X), and subscript ref refers to "reference" conditions (which has been assimilated here to the average "film" conditions, i.e., $\rho_{ref} = \rho_f$). The reference value of the Fick diffusion coefficient D_{ref} appearing in Eq. 4 is defined as

$$D_{ref} \equiv \frac{D_{1,f} \left| \omega_{1,w} - \omega_{1,e} \right| + D_{2,f} \left| \omega_{2,w} - \omega_{2,e} \right|}{\left| \omega_{1,w} - \omega_{1,e} \right| + \left| \omega_{2,w} - \omega_{2,e} \right|} \quad (5)$$

where $D_{1,f}$ is the Fick diffusion coefficient of species 1 (EtOH) in the mixture at average film conditions (see Rosner[4] chapter 3.4.4, Eqs. 3, 4–9)), and where $D_{2,f}$ has been approximated by 2 $D_{1,f}$ for simplicity.

Table 1. Reference Chamber and Spray Composition and Temperature Corresponding to the V-2 Liquid Propellant Rocket of World War II

Pressure	Temperature	Equivalence Ratio	Gas Composition	Initial Liquid Composition
$p = 15$ atm	$T_e = 2970$ K	$\Phi = 1.1$	$w_{2,e} = 0.555$, $w_{3,e} = 1 - w_{2,e}$	$w_1^L\ (t = 0) = 0.75$, $w_2^L\ (t = 0) = 0.25$

In general, a superscript L will be used for any quantity pertaining to the liquid phase, and no superscript will be used for quantities in the gas phase. Thus, $\omega_{1,w}$ is the mass fraction of EtOH at the droplet surface on the gas side.

Single-droplet energy balance and the "wet-bulb" temperature condition

An energy balance condition at the droplet surface provides the corresponding QS-rate law for droplet temperature:

$$(m_1+m_2)c_p^L\frac{dT_w}{dt} = L_1\frac{dm_1}{dt} + L_2\frac{dm_2}{dt} + 4\pi R^2 F(Pe_m)k_f\frac{T_e - T_w}{R} \tag{6}$$

where c_p^L is the prevailing liquid specific heat at constant pressure, L_i are the corresponding latent heats of vaporization, and k is the gas mixture thermal conductivity. A small correction to the energy balance due to the "heat of mixing" is neglected for this high-temperature EtOH + H_2O system.

As mentioned before, in these calculations, it will be assumed that the droplets in the spray attain their stable "wet-bulb" temperature (T_{WB}) on a time scale much shorter than any of the relevant time scales in the problem, i.e., much shorter than the characteristic times for vaporization and exiting the chamber. For instance, this could be easily achieved by preheating the spray to a temperature close to T_{WB}, which is independent of droplet size (as can be seen by inserting $dT_w/dt = 0$ in Eq. 6), before spray injection. In this case, as the droplet composition will not be constant throughout the vaporization process (because EtOH is more volatile than water), the droplet T_{WB} will change as vaporization proceeds. However, as shown below, if the droplet initial temperature is already near T_{WB} (corresponding to initial composition), then the droplet temperature remains equal (to a very good approximation) to the time-dependent T_{WB} throughout the entire vaporization lifetime.

Choice of dimensionless variables

Assuming that the spray is injected in the chamber at the (size-independent) wet-bulb temperature, through the Vapor-liquid equilibrium (VLE) condition

$$x_i^L\ \gamma_i\ p_i^{sat} = x_{i,w}\ p \tag{7}$$

(where x_i, γ_i, and p_i^{sat} are the mole fraction, activity coefficient, and saturation pressure of species i, and p is the constant chamber pressure), we see that the gas-phase composition at the droplet interface becomes a function of droplet composition only. Hence, given the exterior (far-field) gas composition and temperature, the film average conditions become fully determined also as a function of droplet composition.

Consequently, the former rate laws for the droplet state variables m_1 and m_2 factorize as the droplet radius R times a function of droplet composition only. This factorization enables a straightforward analytical integration of the PBE that determines the steady-state DSD function in the combustor (see below). For this reason, it is convenient to use the droplet composition (described here by the EtOH mass fraction, ω) as one of the internal variables of the spray. The second (size-related) internal variable has been chosen here as the droplet total mass ($m \equiv m_1 + m_2$). This choice is a consequence of the "feed" spray, approximated here by a log-normal distribution in droplet volume (hence, also log-normal in droplet mass, assuming that the feed is at a constant temperature).

The last equation, needed to close the system, is the rate law for droplet size. This can be readily derived by inserting Eqs. 1,2, and 6 in the time derivative of

$$m = \frac{4\pi}{3}\ R^3\ \rho^L \tag{8}$$

where the liquid density ρ^L is given below as a function of droplet temperature and composition (see Eq. 23).

As the complexity of the former (quite simplified) system precludes an analytical solution, it seems convenient to perform all the needed numerical calculations using dimensionless variables (of order unity), defined using their corresponding characteristic scales (subscript ref, except for D_{ref} where subscript ref_0 will be used). The dimensionless variables used here are defined by:

Length: $R_{ref} \equiv d_{32}/2$ $\quad a \equiv R/R_{ref}$

Temperature: $T_{ref} \equiv T_{b,1}$ $\quad \theta \equiv T/T_{ref}$

Liquid density: $\rho_{ref}^L \equiv \rho^L$(at const. ref. liq. cond.)

$\varrho^L \equiv \rho^L/\rho_{ref}^L$

Gas density: $\rho_{ref} \equiv \rho$(at const. ref. gas cond.)

$\varrho \equiv \rho/\rho_{ref}$

Mass: $m_{ref} \equiv \frac{4\pi}{3}R_{ref}^3\rho_{ref}^L$ $\quad \mu_i \equiv m_i/m_{ref}$

Fick diffusion coefficient:

$D_{ref_0} \equiv D_{ref}$(at const. ref. gas cond.)

$d \equiv D_{ref}/D_{ref_0}$

$\delta_i \equiv D_{i,f}/D_{ref}$

Time: $t_{ref} \equiv \frac{1}{3}\frac{\rho_{ref}^L}{\rho_{ref}}\frac{R_{ref}^2}{D_{ref_0}}$ $\quad \tau \equiv t/t_{ref}$

Specific energy: $L_{ref} \equiv L_1(T = T_{b,1})$ $\quad \mathcal{L}_i \equiv L_i/L_{ref}$

$c \equiv c_p/(L_{ref}/T_{ref})$

Fourier thermal conductivity: $k_{ref} \equiv D_{ref_0}\rho_{ref}L_{ref}/T_{ref}$

$\lambda \equiv k/k_{ref}$

In the former definitions, "const. ref. gas/liq. cond." correspond to the boiling temperature of EtOH at the prevailing pressure ($T_{b,1}$), initial droplet composition (for the liquid phase) and exterior (far-field) reference gas composition and temperature for the gas phase, given by Table 1, with composition at the droplet interface given by the VLE condition.

Note that the reference temperature, defined as the boiling temperature of pure EtOH at the prevailing pressure, is not equal to the initial droplet temperature. This way the reference temperature has the correct order of magnitude, but does not depend on droplet initial composition or initial temperature, facilitating fast comparison between numerical results computed with different initial compositions or temperatures (but with the same pressure). As a consequence of this choice ρ^{L}_{ref} is slightly different from the initial droplet density.

In terms of these variables, the rate laws for m_1 and m_2 take the form

$$\dot{\mu}_1 = -a\, F(Pe_m)\, \varrho d \cdot \left(B_m\, \omega_{1,w} + \delta_1\left(\omega_{1,w} - \omega_{1,e}\right)\right) \quad (9)$$

$$\dot{\mu}_2 = -a\, F(Pe_m)\, \varrho d \cdot \left(B_m\, \omega_{2,w} + \delta_2\left(\omega_{2,w} - \omega_{2,e}\right)\right) \quad (10)$$

where $\dot{}$ denotes $d/d\tau$.

The dimensionless form of the rate law for droplet temperature is

$$(\mu_1 + \mu_2)c^{L}\dot{\theta}_w = a\, F(Pe_m)\, \varrho d \cdot \left(\frac{\lambda}{\varrho d}(\theta_e - \theta_w) + \mathcal{L}_1 \frac{\dot{\mu}_1}{a\, F(Pe_m)\, \varrho d} + \mathcal{L}_2 \frac{\dot{\mu}_2}{a\, F(Pe_m)\, \varrho d}\right) \quad (11)$$

where the $\dot{\mu}_i$ are given by Eqs. 9 and 10.

Finally, the time evolution of the droplet size is given, in dimensionless form, by

$$\dot{a} = \frac{a}{3} \cdot \left(\frac{\dot{\mu}_1 + \dot{\mu}_2}{\mu_1 + \mu_2} - \frac{\dot{\varrho}^{L}}{\varrho^{L}}\right) \quad (12)$$

where the time derivative of the dimensionless liquid density ϱ^{L} can be determined in terms of μ_i and θ_w by the corresponding equation of state (EOS) of the liquid phase (Eq. 23) and Eqs. 9–11.

Population balance equation governing the spray evolution

Inspection of the rate laws for μ_1 and μ_2 (Eqs. 9 and 10) shows that all the dependence on droplet size is contained in the factor $a \propto \mu^{1/3}$ (where $\mu \equiv \mu_1 + \mu_2$ is the dimensionless total mass). On the other hand, taking into account the VLE boundary condition at the droplet interface and assuming that all droplets are at T_{WB}, we see that $\dot{\mu}_i/a$ is a function of droplet composition alone, justifying our choice of dimensionless variables.

To derive the PBE that governs the evolution of the spray, we need to write the corresponding rate laws for the variables used to describe the spray population: μ and ω. The corresponding rate laws for droplet mass and composition can be easily derived from their definitions

$$\mu \equiv \mu_1 + \mu_2, \quad \omega \equiv \frac{\mu_1}{\mu_1 + \mu_2} \quad (13)$$

hence

$$\dot{\mu} = \dot{\mu}_1 + \dot{\mu}_2, \quad \dot{\omega} = \frac{\dot{\mu}_1 - \omega\dot{\mu}}{\mu} \quad (14)$$

According to the former rate laws $\dot{\mu} \leq 0$ and $\dot{\omega} \leq 0$, corresponding to a vaporization process in which the water mass fraction within the droplet increases (because EtOH is more volatile than water). In a similar way, we remark that

$$\dot{\mu}|_{\mu=0,\ \omega\neq 0} = \dot{\omega}|_{\mu=0,\ \omega\neq 0} = \dot{\omega}|_{\mu\neq 0,\ \omega=0} = 0 \quad (15)$$

which means that as $\mu \to 0$ the EtOH mass fraction of the droplets also vanishes. As will be shown later, this causes the steady-state NDDF of the spray to become strongly peaked in the region $\omega \simeq 0$.

The PBE that determines the steady-state NDDF of the spray in the chamber in this case takes the form of the following first order, linear PDE:

$$\frac{n - n_F}{Dam} + \frac{\partial(\dot{\mu}n)}{\partial\mu} + \frac{\partial(\dot{\omega}n)}{\partial\omega} = 0 \quad (16)$$

where n is the NDDF of the spray, and n_F the corresponding NDDF of the "feed" spray, both of them as a function of the droplet state variables: mass and composition. Hence, the total number of droplets per unit volume in the combustion chamber (N) and in the "feed" (N_F) are given, respectively, by

$$N = \int_0^{\infty}\int_0^{\omega_F} n(\mu,\omega)\, d\mu\, d\omega \quad (17)$$

$$N_F = \int_0^{\infty}\int_0^{\omega_F} n_F(\mu,\omega)\, d\mu\, d\omega \quad (18)$$

where ω_F is the initial mass fraction of EtOH in the spray, which remains the maximal possible value of ω at all times.

The parameter *Dam* in the former PBE is a *vaporization* Damköhler number, defined as the ratio of the characteristic residence time in the chamber to the characteristic vaporization time (defined here as t_{ref}).

Boundary Conditions. The solution of this PDE is not unique until the appropriate conditions are imposed at the boundaries of the integration domain. In our case, these conditions are related to the rate at which the droplets enter the integration domain $\omega \in [0, 1]$, $\mu \in [0, \infty)$. On one hand, it is clear that $n(\omega, \mu \to \infty) = 0$. On the other hand, the condition needed for integration with respect to the ω variable can be derived from the feed NDDF n_F, assuming the feed is Dirac-delta-like with respect to droplet composition (with a certain $\omega = \omega_F$) we have

$$n_F(\mu,\omega)\, d\mu\, d\omega = n_F(\mu)\, \delta(\omega - \omega_F)\, d\mu\, d\omega \quad (19)$$

Hence, integrating Eq. 16 with respect to ω between $\omega_F - d\omega$ and $\omega_F + d\omega$, in the limit $d\omega \to 0$ we find

$$-\frac{n_F(\mu)}{Dam} + \dot{\omega}n|_{\omega=\omega_{F_+}} - \dot{\omega}n|_{\omega=\omega_{F_-}} = 0 \quad (20)$$

Then, as $\dot{\omega} < 0$ and the input spray is a Dirac delta at ω_F, we have that $n\ (\omega > \omega_F) = 0$. In this way, we find the feed condition

$$n(\mu,\omega_F) = -\frac{n_F(\mu)}{Dam\ \dot{\omega}(\mu,\omega_F)} \quad (21)$$

which has been used in solving Eq. 16. In the integration domain, $0 \leq \omega < \omega_F$ Eq. 16 takes the simpler form

Table 2. Basic Property Data Used in this Study

Property		Ethanol	Water	CO_2	Oxygen
Molecular weight	M (kg/kmol)	46.07	18.016	44.011	32.0
Critical point	ρ_c (kg/m^3)	274.2	321.7	468.2	437.1
	T_c (K)	513.9	647.1	304.2	154.6
	p_c (atm)	62.18	217.7	72.8	49.8
	Z_c	0.248	0.229	0.274	0.288
Specific heat (gas)	c_p (J/(kg K))	$73.55\ T^{0.5381}$	$438.6\ T^{0.2409}$	$188.6\ T^{0.2698}$	$392.0\ T^{0.1472}$
Specific heat (liq.)	c_p (J/(kg K))	$2400\ (T/300)^{1.170}$	$4180\ (T\ /\ 300)^{0.121}$		1693
Antoine equation data	$\mathcal{A}$	8.32109	7.96681		6.69144
	$\mathcal{B}$ (K)	1718.10	1668.21		319.013
	$\mathcal{C}$ (K)	35.63	45.15		6.453

$$\frac{n}{Dam}+\frac{\partial(\dot{\mu}n)}{\partial\mu}+\frac{\partial(\dot{\omega}n)}{\partial\omega}=0 \tag{22}$$

Choices of basic property data and operating conditions

To solve the former bivariate-PBE, one also needs to specify all thermo-physical properties of both mixtures considered (spray and surrounding gas) as well as the operating conditions. In this respect, the liquid fuel spray is assumed to be composed of EtOH and water, and the liquid oxidizer spray (which is assumed to vaporize ''instantaneously'' (see below)) is composed of pure oxygen. The surrounding gas, which is considered as a mixture of ideal gases (the constant chamber pressure is taken to be $p = 15$ atm), is composed of any unreacted EtOH (subscript 1), water (subscript 2), CO_2 (subscript 3), and oxygen (subscript 4).

The constant ''reference'' chamber conditions used both for illustrative calculations under prescribed chamber conditions, as well as the starting point for the iterative procedure used to solve the coupled (spray-chamber) PBE, correspond to the historically important case of the V-2 chemical rocket (see Table 1).

The specific heats of the pure components in the gas phase have been approximated, in the range of temperatures of interest, as power-laws in absolute temperature (see Table 2), computed based on available data.[6] Specific heats of the pure components in the liquid phase were also approximated by power-laws, in the calculation of the specific heat of the liquid mixture the enthalpy-of-mixing was neglected.

While the gas phase is well-described by the ideal gas EOS, the liquid mixture is non ideal and its density has been a approximated by the relation

$$\rho^{\mathrm{L}}(\mathrm{kg/m^3})=\left(\frac{x_1}{\rho_1^{\mathrm{L}}}+\frac{x_2}{\rho_2^{\mathrm{L}}}-4x_1x_2 0.045\times 10^{-3}\right)^{-1} \tag{23}$$

where x_i are the mole fractions of EtOH and water in the liquid phase and ρ_i^{L} are the corresponding pure-component saturated liquid densities, estimated from:

$$\rho_i^{\mathrm{L}}=\frac{\rho_{\mathrm{ref},i}}{Z_i^{\left(1-(T/T_{\mathrm{c},i})\right)^{n_i}}} \tag{24}$$

In the case of EtOH the parameters ρ_{ref} and Z are the critical density and critical compressibility factor (see Table 2) and the exponent is taken to be $n_1 = 0.325$, whereas for water, more accurate results were found using the values $\rho_{\mathrm{ref},2} = 347.1$ kg/m^3 and $Z_2 = 0.274$ with $n_2 = 0.286$.

The bubble point temperature of the EtOH + water mixture, as a function of $\omega(T_b(\omega))$ at the prevailing constant chamber pressure, has been computed solving for T the VLE-condition (Eq. 7) together with the normalization condition, i.e.,

$$\sum_{i=1}^{2} x_i^{\mathrm{L}}\ \gamma_i\ \frac{p_i^{\mathrm{sat}}}{p}=1 \tag{25}$$

where the saturation pressure of each pure component is given, as a function of temperature, by the 3-parameter Antoine equation

$$\log_{10}\left(p_i^{\mathrm{sat}}/\mathrm{Torr}\right)=\mathcal{A}-\frac{\mathcal{B}}{T-\mathcal{C}} \tag{26}$$

with parameters $\mathcal{A}$, $\mathcal{B}$, and $\mathcal{C}$ given in Table 2, and where the activity coefficients have been computed using a Van Laar model.[7] with parameters fitted using the azeotrope VLE data of Ref. 8. As numerical evaluation of the mixture bubble point temperatures, at different EtOH mass fractions, is needed a significant number of times for each particular case, and solving Eq. 25 is time consuming, the function $T_b(\omega)$ has been approximated by polynomial interpolation based on 50 Chebyshev nodes[9] for ω in the interval [0, 1]. For each of the nodes considered the corresponding value of $T_b(\omega)$ was computed solving Eq. 25, this strategy produces an approximation to the function $T_b(\omega)$ which is extremely accurate and, at the same time, very fast to evaluate.

Regarding the phase change and combustion specific heats, the vaporization latent heats of the pure components have been approximated by the power laws

$$L_i=L_{\mathrm{ref},i}\cdot\left(1-\frac{T}{T_{\mathrm{c},i}}\right)^{n_i} \tag{27}$$

with $L_{\mathrm{ref},1} = 0.9177$ MJ/kg, $n_1 = 0.079$ for EtOH; $L_{\mathrm{ref},2} = 2.8893$ MJ/kg, $n_2 = 0.321$ for water; and $L_{\mathrm{ref},4} = 0.2130$ MJ/kg, $n_4 = 0$ for oxygen. The lower heat of combustion of pure EtOH in the liquid phase is taken to be 26.82 MJ/kg.

Regarding transport properties of the gas phase, the mixture thermal conductivity has been approximated by a cube-root law (see Eq. 3.3–7 of Ref. 4, p 114), where the thermal conductivities of the pure gas phase components have been approximated by power-laws in the local temperature

$$k_i = k_{\mathrm{ref},i}\left(\frac{T}{1000}\right)^{n_i} \tag{28}$$

with $k_{\mathrm{ref},1} = 0.1231$ W/(mK), $n_1 = 1.74$ for EtOH; $k_{\mathrm{ref},2} = 0.0880$ W/(mK), $n_2 = 1.27$ for water; $k_{\mathrm{ref},3} = 0.0665$ W/(mK), $n_3 = 0.95$ for CO_2; and $k_{\mathrm{ref},4} = 0.0740$ W/(mK), $n_4 = 0.80$ for oxygen.

Finally, the effective Fick diffusion coefficient of EtOH in the gas mixture (D_1) has been computed using the additive-resistance formula (see Eq. 3.4–9 of Ref. 4, p. 120), where the participating binary Fick diffusion coefficients have been approximated by a functional form suggested by the kinetic theory of ideal gases

$$D_{1i} = \frac{D_{\mathrm{ref},1i}}{p(\mathrm{atm})}\left(\frac{T}{1000}\right)^{1.75} \tag{29}$$

with $D_{\mathrm{ref},12} = 0.732 \times 10^{-4}$ m^2/s, $D_{\mathrm{ref},13} = 0.672 \times 10^{-4}$ m^2/s and $D_{\mathrm{ref},14} = 1.040 \times 10^{-4}$ m^2/s. For present purposes, the effective Fick diffusion coefficient of water in the gas mixture has been approximated by $D_2 \simeq 2\,D_1$.

Theoretical Development: Choice of Mathematical and Numerical Methods

Analytic solution of the PBE by the method of characteristics

To solve the PBE as written in Eq. 22, using the method of characteristics, one would be forced to calculate derivatives of the rate laws $\dot{\mu}$ and $\dot{\omega}$ with respect to the independent variables μ and ω, yielding a set of complicated analytical expressions that would make this method very time consuming. However, according to the former rate laws $\dot{\mu} \propto \mu^{1/3}$ and $\dot{\omega} \propto \mu^{-2/3}$. Hence, we may define

$$\dot{\mu} \equiv -\mu^{1/3}\,A, \quad \dot{\omega} \equiv -\mu^{-2/3}\,B \tag{30}$$

where the functions A and B depend only on liquid-phase composition ω. Inserting these definitions in Eq. 22, we find

$$\frac{\mu A}{B}\frac{\partial}{\partial \mu}\left(\mu^{1/3} B\, n\right) + \frac{\partial}{\partial \omega}\left(\mu^{1/3} B\, n\right) = \frac{\mu\, n}{Dam} \tag{31}$$

which is ready to be solved for $\mu^{1/3}\,B\,n$ using the method of characteristics directly. This form of the PBE is particularly convenient because it suggests the use of EtOH mass fraction in the liquid phase (ω) as the coordinate along characteristic paths. On the other hand, from Eq. 31, we find that the total mass along characteristic paths is given by

$$\mu(\omega) = \mu_0 \cdot \exp\left(-\int_{\omega}^{\omega_{\mathrm{F}}} \frac{A}{B}\, d\omega\right) \tag{32}$$

where $\mu_0 = \mu(\omega_{\mathrm{F}})$. This results shows clearly that all characteristic paths (corresponding to initial conditions $(\mu, \omega) = (\mu_0, \omega_{\mathrm{F}})$) leave the domain of integration through the origin $(\mu, \omega) = (0, 0)$. This is because B vanishes proportionally to ω as $\omega \to 0$. Accordingly, the solution for $\mu^{1/3}\,B\,n$ along the characteristic paths is given by

$$\mu^{1/3} B\, n = \mu_0^{1/3} B_0\, n_0 \cdot \exp\left(-\frac{1}{Dam}\int_{\omega}^{\omega_{\mathrm{F}}} \frac{\mu^{2/3}}{B}\, d\omega\right) \tag{33}$$

where $\mu = \mu(\omega)$ is given by Eq. 32, $B_0 = B(\omega_{\mathrm{F}})$ and $n_0 = n(\mu_0, \omega_{\mathrm{F}})$. Recalling the "boundary" condition Eq. 21, we find the solution for the steady state NDDF:

$$n[\mu(\mu_0,\omega),\omega] = \frac{\mu_0\, n_{\mathrm{F}}(\mu_0)}{Dam\;\mu(\mu_0,\omega)^{1/3}\,B} \times \exp\left(-\frac{1}{Dam}\int_{\omega}^{\omega_F} \frac{\mu(\mu_0,\omega)^{2/3}}{B}\, d\omega\right) \tag{34}$$

where $\mu(\mu_0, \omega)$ is given by Eq. 32.

Calculation of quantities of interest

The method of characteristics provides the solution of the PBE $n\ (\mu, \omega)$ in parametric form, in terms of the initial condition for μ along each characteristic path (μ_0), and the coordinate along the characteristic paths (ω). However, we will be mainly interested in the moments of n, or the average values of certain functions $K\ (\mu, \omega)$

$$\langle K\rangle = \frac{1}{N}\int_0^{\infty}\int_0^{\omega_{\mathrm{F}}} K(\mu,\omega)\; n(\mu,\omega)\; d\mu\; d\omega \tag{35}$$

based on the normalized NDDF n/N.

The calculation of these average values can be easily done in terms of $n\ (\mu_0, \omega)$ taking into account the fact that the Jacobian of the transformation $\{\mu, \omega\} \to \{\mu_0, \omega'\}$ with

$$\mu_0 = \mu \cdot \exp\int_{\omega}^{\omega_{\mathrm{F}}} \frac{A}{B}\, d\omega, \qquad \omega' = \omega \tag{36}$$

is just μ/μ_0. Hence, for any $K\ (\mu, \omega)$

$$\langle K\rangle = \frac{1}{N}\int_{-\infty}^{\infty}\int_0^{\omega_F} K[\mu(\mu_0,\omega),\omega]\;\mu(\mu_0,\omega) \cdot n(\mu_0,\omega)\; d\ln\mu_0\; d\omega \tag{37}$$

where

$$\mu(\mu_0,\omega)\; n(\mu_0,\omega) = \frac{\mu(\mu_0,\omega)^{2/3}}{Dam\;B}\cdot \mu_0\; n_{\mathrm{F}}(\mu_0)\cdot \times \exp\left(-\frac{1}{Dam}\int_{\omega}^{\omega_{\mathrm{F}}} \frac{\mu(\mu_0,\omega)^{2/3}}{B}\, d\omega\right) \tag{38}$$

In particular, we will be interested in certain mixed moments of the spray normalized NDDF $\langle \mu^{\alpha}\omega^{\beta}\rangle$, defined by

$$\left\langle \mu^{\alpha}\omega^{\beta}\right\rangle \equiv \frac{1}{N}\int_{-\infty}^{\infty}\int_0^{\omega_{\mathrm{F}}} \mu^{\alpha}\omega^{\beta}\;\mu\; n\; d\ln\mu_0\; d\omega \tag{39}$$

where $\mu\, n$ is given by Eq. 38 and μ by Eq. 32.

Coupling Between the Dispersed (Fuel Spray) and Continuous Phases; Self-Consistent Steady-State Chamber Composition and Temperature

To solve the PBE that governs the spray population one needs to know T_{WB} as a function of droplet composition as well as the vaporization rates of EtOH and water all of which depend on the chamber temperature and composition. However, conditions in the combustion chamber should be consistent with the mass and energy supplied by the

combustion of fuel resulting from the vaporization of the steady state population of fuel droplets present in the chamber. This condition couples the calculation of the steady-state spray distribution function with the calculation of the ambient conditions in the chamber, resulting in a highly nonlinear problem.

An iterative strategy is adopted to solve this nonlinear problem, as explained below. The iterative scheme starts with the calculation of $n(\mu, \omega)$ corresponding to the reference (prespecified) values of chamber temperature and composition (Table 1), solving Eq. 22 with "boundary" condition Eq. 21 as shown in the previous section. Once the spray NDDF $n(\mu, \omega)$ is known, the corrected chamber temperature and composition are computed according to the mass and energy balance shown below. Then, the wet-bulb temperature $T_{WB}(\omega)$ and rate laws $\dot{\mu}(\mu, \omega)$ and $\dot{\omega}(\mu, \omega)$ corresponding to the new (corrected) ambient conditions are computed. Once this is done, solving again the PBE (Eq. 22), we find the new spray NDDF $n(\mu, \omega)$, corresponding to corrected values of the chamber composition and temperature, and we are ready for the next iteration. This process is repeated until convergence is achieved.

The mass- and energy-balance equations that relate ambient chamber conditions to the steady-state spray distribution function are explained below.

Mass balance

The first set of variables needed to describe the mass balance are the total in and out mass flow rates in the combustion chamber: We define $\dot{m}_F^{in}$ ($\dot{m}_4^{in}$) as the total mass of fuel spray (respectively oxidizer (O_2)) entering the chamber per unit time and per unit chamber volume. Accordingly, we define $\dot{m}_S^{out}$ as the total mass of "unvaporized" fuel spray leaving the chamber per unit time and per unit chamber volume. Finally, $\dot{m}_V^{out}$ denotes the total mass of vapor leaving the chamber per unit time and per unit chamber volume.

Besides the overall mass-flow rates, we need to specify the rates at which each species is supplied to the vapor phase in the chamber. For this purpose, we define I_1 (I_2) as the total mass of EtOH (water) supplied to the vapor phase by spray vaporization, per unit time and per unit chamber volume, respectively. Given the vaporization rate laws for EtOH and water ($\dot{m}_1$ and $\dot{m}_2$), once the steady-state spray NDDF $n(\mu, \omega)$ is known, I_1 and I_2 can be computed according to

$$I_i = \int\int -\dot{m}_i \, n \, d\mu \, d\omega \tag{40}$$

where the double integral is performed over all possible values of μ and ω. We also assume that all the oxygen supplied to the chamber ($\dot{m}_4^{in}$) vaporizes instantaneously and that no other chemical species enter the chamber.

On the other hand, the average mass fraction of EtOH in the spray in the chamber ($\overline{\omega}$) is given in terms of the steady-state number density population $n(\mu, \omega)$ by

$$\overline{\omega} = \frac{\int\int \mu \, \omega \, n \, d\mu \, d\omega}{\int\int \mu \, n \, d\mu \, d\omega} \tag{41}$$

The quantities I_i and $\overline{\omega}$ have to be updated at each iteration, whereas the average mass fraction of EtOH in the feed spray (ω_F) has a constant value.

Regarding the combustion chamber gas phase composition, we recall that the chamber is considered "well-mixed." Hence, the composition is determined by the external (far-field—from the viewpoint of the spray droplets) mass fractions $\omega_{i,e}^V$. On the other hand, in this section it will be assumed that the combustion process takes place under "fuel-lean" conditions. As a consequence, the exterior vapor-phase mass fraction of fuel vanishes ($\omega_{1,e}^V = 0$).

Once all the variables that enter the mass-balance have been defined, the mass balance conditions are specified by

$$\dot{m}_F^{in} \, \omega_F = I_1 + \dot{m}_S^{out} \, \overline{\omega} \tag{42}$$

$$\dot{m}_F^{in} \cdot (1 - \omega_F) = I_2 + \dot{m}_S^{out} \cdot (1 - \overline{\omega}) \tag{43}$$

$$\dot{m}_4^{in} = \dot{m}_F^{in} \cdot \frac{\omega_F}{f_{stoich} \Phi} \tag{44}$$

$$\frac{f_{stoich,2}}{f_{stoich}} I_1 + I_2 = \dot{m}_V^{out} \, \omega_{2,e}^V \tag{45}$$

$$\frac{f_{stoich,3}}{f_{stoich}} I_1 = \dot{m}_V^{out} \, \omega_{3,e}^V \tag{46}$$

$$-\frac{1}{f_{stoich}} I_1 + \dot{m}_4^{in} = \dot{m}_V^{out} \, \omega_{4,e}^V \tag{47}$$

$$\omega_{2,e}^V + \omega_{3,e}^V + \omega_{4,e}^V = 1 \tag{48}$$

where the indicated stoichiometric ratios correspond to the chemical reaction

$$C_2H_5OH + 3O_2 = 2CO_2 + 3H_2O \tag{49}$$

are given by

$$\begin{aligned} f_{stoich} &= \frac{M_{C_2H_5OH}}{3M_{O_2}} = 0.4799 \\ f_{stoich,2} &= \frac{M_{H_2O}}{M_{O_2}} = 0.5630 \\ f_{stoich,3} &= \frac{2M_{CO_2}}{3M_{O_2}} = 0.9169 \end{aligned} \tag{50}$$

The two first equations (Eqs. 42 and 43) simply state the in/out mass balance for the fuel spray. Equation 44 determines the oxygen (in-) flow rate in terms of the fuel (in-) flow rate, where the equivalence ratio Φ has a prespecified (constant) value (for the V-2 rocket the feed- value considered was $\Phi = 1.1$). Equations 45–47 state the balance of H_2O, CO_2, and O_2 produced (or consumed) by the chemical reaction (per unit time and unit chamber volume). In these equations, we have assumed that, because the chamber operates under steady- and fuel-lean conditions, the rate at which the fuel is supplied to the vapor phase I_1 is equal to the rate of fuel consumption by homogeneous chemical reactions. The last equation (Eq. 48) is also a consequence of our assumption of evaporation-rate-controlled combustion under fuel-lean conditions (i.e., $\omega_{1,e}^V = 0$).

Note that the sum of Eqs. 42 and 43 gives the overall mass balance of the fuel spray:

$$\dot{m}_F^{in} = I_1 + I_2 + \dot{m}_S^{out} \tag{51}$$

Similarly, the sum of Eqs. 45–47 gives the overall mass balance of the vapor in the chamber:

$$I_1 + I_2 + \dot{m}_4^{\text{in}} = \dot{m}_V^{\text{out}} \tag{52}$$

Finally, adding these two last equations, we obtain the total mass conservation equation, as expected

$$\dot{m}_F^{\text{in}} + \dot{m}_4^{\text{in}} = \dot{m}_S^{\text{out}} + \dot{m}_V^{\text{out}} \tag{53}$$

At each iteration, once the steady-state NDDF of the spray in the chamber $n(\mu, \omega)$ is known, the values of I_i and $\overline{\omega}$ can be computed via quadratures over $n(\mu, \omega)$. Then, the corresponding vapor phase composition in the chamber ($\omega_{2,e}^V$, $\omega_{3,e}^V$ and $\omega_{4,e}^V$), as well as the corresponding in/out mass flow rates ($\dot{m}_F^{\text{in}}$, $\dot{m}_4^{\text{in}}$, $\dot{m}_S^{\text{out}}$ and $\dot{m}_V^{\text{out}}$) are determined by the former system (Eqs. 42–48).

It is also noteworthy that, at each iteration (once $n(\mu, \omega)$ is known), the former mass balance can be easily solved independently of the (slightly more involved) energy balance, which determines the chamber temperature T_e as explained below.

Energy balance

Assuming steady-state operation and adiabatic conditions, the energy conservation equation equates the chemical energy released to the energy needed for heating and vaporization of the O_2(L) and fuel sprays as well as heating of the resulting fuel and oxidizer vapors.

For vaporization-controlled combustion, the energy released by the chemical reaction per unit time and per unit chamber volume is given by

$$\dot{q}_{\text{chem}} = I_1\, Q_1 \tag{54}$$

where Q_1 is the lower heat of combustion of EtOH in vapor phase ($Q_1 = L_1 + 26.82$ MJ/kg).

Assuming that the liquid oxygen is injected in the chamber at $T = T_{0,O_2(L)} = 90$ K, and that it vaporizes at $T = T_{b,O_2(L)}$, the total energy needed (per unit time and per unit chamber volume) for oxidizer vaporization and heating up to the wet-bulb temperature of the feed fuel spray ($T_{WB}(\omega_F) \equiv T_F$) can be expressed:

$$\dot{q}_{O_2(L)} = \dot{m}_4^{\text{in}}\Big(\int_{T_{0,O_2(L)}}^{T_{b,O_2(L)}} c_{p,O_2(L)}\, dT + L_4 + \int_{T_{b,O_2(L)}}^{T_F} c_{p,4}\, dT\Big) \equiv \dot{m}_4^{\text{in}}\, L_{4,\text{eff}} \tag{55}$$

where L_4 is the heat of vaporization of the O_2(L), $c_{p,O_2(L)}$ is the specific heat of the O_2(L), $c_{p,4}$ is the specific heat the of the oxidizer in the vapor phase, and where we have defined $L_{4,\text{eff}}$ as the "effective" O_2(L) heat of vaporization.

The energy needed for fuel spray heating and vaporization, per unit time and per unit chamber volume, is given by

$$\dot{q}_F = I_1\, L_{F,1} + I_2\, L_{F,2} + \int\int \big(-L_1'\, \dot{m}_1 - L_2'\, \dot{m}_2 + c_{p,F}^L\, T_{WB}'\, m\, \dot{\omega}\big) n\, d\mu\, d\omega \tag{56}$$

where $L_{F,i}$ is the heat of vaporization of component i at the wet-bulb temperature of the feed spray ($L_{F,i} \equiv L_i\,(T_F)$).

In the former Eq. 56, the first two terms are dominant, representing the energy needed for vaporization of the fuel spray assuming that the vaporization takes place at the initial wet-bulb temperature of the feed spray (T_F). The third term in Eq. 56 is a small correction, accounting for the heating of the fuel spray from its initial temperature up to the composition-dependent T_{WB} as well as for the variation of the heats of vaporization produced by this temperature change. In this last term, L_i' is the difference between the vaporization latent heat corresponding to the temperature at which the vaporization occurs and the vaporization latent heat at the initial wet-bulb temperature

$$L_i' \equiv L_i(T_{WB}[\omega]) - L_{F,i} \tag{57}$$

On the other hand $c_{p,F}^L$ is the specific heat of the fuel spray:

$$c_{p,F}^L = c_{p,1}^L \omega + c_{p,2}^L (1 - \omega) \tag{58}$$

and T_{WB}' is defined as the variation of the (size-independent) wet-bulb temperature of the droplets with respect to composition

$$T_{WB}' \equiv \frac{dT_{WB}(\omega)}{d\omega} \tag{59}$$

Finally, the energy needed, per unit time and per unit chamber volume, for vapor heating up to the chamber temperature (T_e) is given by

$$\dot{q}_h = \int_{T_F}^{T_e} (I_1 c_{p,1} + I_2 c_{p,2} + \dot{m}_4^{\text{in}} c_{p,4}) dT - \dot{q}_h' \tag{60}$$

where the first three terms, which dominate, represent the energy needed for vapor heating from the initial temperature T_F, and where the last term is a small correction that accounts for the difference between T_F and the actual (composition-dependent) wet-bulb temperature at which the vaporization of EtOH and water takes place. This small correction is given by

$$\dot{q}_h' = \int\int \left[\int_{T_F}^{T_{WB}(\omega)} \left(-\dot{m}_1\, c_{p,1} - \dot{m}_2\, c_{p,2}\right) dT \right] n\, d\mu\, d\omega \tag{61}$$

Having evaluated all terms entering the energy balance, the overall energy conservation equation becomes:

$$\dot{q}_{O_2(L)} + \dot{q}_F + \dot{q}_h = \dot{q}_{\text{chem}} \tag{62}$$

Recalling the former mass-balance equations (Eqs. 42–48), the energy-balance equation can be written simply as

$$I_1\, h_1(T_e) + I_2\, h_2(T_e) + \dot{m}_4^{\text{in}}\, h_4(T_e) = \dot{m}_F^{\text{in}}\, Q_{F,\text{eff}}^{\text{in}} - \dot{m}_S^{\text{out}}\, Q_{F,\text{eff}}^{\text{out}} + \dot{q}' \tag{63}$$

where we have defined $h_i(T_e)$ as the specific enthalpy of component i in the vapor phase at chamber temperature T_e minus the corresponding value at T_F:

$$h_i(T) \equiv \int_{T_F}^{T} c_{p,i}\, dT \tag{64}$$

we have defined $Q_{F,\text{eff}}^{\text{in}}$ as the "effective" heat of combustion (under the present operating conditions) of the feed fuel spray, and $Q_{F,\text{eff}}^{\text{out}}$ as the "effective" heat of combustion of the fuel spray that leaves the chamber without being vaporized:

$$Q^{\text{in}}_{\text{F,eff}} \equiv \omega_{\text{F}}\left(Q_1 - L_{\text{F},1}\right) - \left(1-\omega_{\text{F}}\right) L_{\text{F},2} - \frac{\omega_{\text{F}} L_{4,\text{eff}}}{f_{\text{stoich}}\Phi}$$
$$Q^{\text{out}}_{\text{F,eff}} \equiv \overline{\omega}\left(Q_1 - L_{\text{F},1}\right) - \left(1-\overline{\omega}\right) L_{\text{F},2} \quad (65)$$

Finally, in the former Eq. (63), we have also defined $\dot{q}'$ as the extra term that accounts for the difference in vaporization heats and specific enthalpies related to the difference between the feed fuel spray wet-bulb temperature (T_{F}) and the actual (composition-dependent) wet-bulb temperature at which the vaporization takes place. This term, (a small correction), is given by:

$$\dot{q}' \equiv \int\int \left[-\left(h_1[T_{\text{WB}}(\omega)] - L'_1\right)\cdot \dot{m}_1 - \left(h_2[T_{\text{WB}}(\omega)] - L'_2\right)\cdot \dot{m}_2 - c^{L}_{\text{p},F}\, T'_{\text{WB}}(\omega)\, m\, \dot{\omega}\right] n\, d\mu\, d\omega \quad (66)$$

where $\dot{m}_{\text{i}}$ and $\dot{\omega}$ denote the dimensional quantities dm_{i}/dt and $d\omega/dt$. The mass and energy balance equations in terms of suitable dimensionless units are introduced in the following section.

Mass and energy balance in dimensionless form

For the development below, we define the characteristic number of droplets per unit volume in the feed spray (N_{F}) as the number density corresponding to the dimensionless mass rates per unit time and per unit chamber volume. Hence, we introduce the dimensionless mass flow rates

$$\dot{\mu}^{\text{in/out}}_k = \dot{m}^{\text{in/out}}_k \cdot \frac{t_{\text{ref}}}{N_{\text{F}}\, m_{\text{ref}}}, \quad j_i = I_i \cdot \frac{t_{\text{ref}}}{N_{\text{F}}\, m_{\text{ref}}} \quad (67)$$

where subscript k takes values F and 4 in the case of in-flows (superscript in), and values S and V in the case of out-flows (superscript out). Thus, the dimensionless mass-balance system becomes:

$$\dot{\mu}^{\text{in}}_{\text{F}}\, \omega_{\text{F}} = j_1 + \dot{\mu}^{\text{out}}_{\text{S}}\, \overline{\omega} \quad (68)$$
$$\dot{\mu}^{\text{in}}_{\text{F}} \cdot \left(1-\omega_{\text{F}}\right) = j_2 + \dot{\mu}^{\text{out}}_{\text{S}} \cdot \left(1-\overline{\omega}\right) \quad (69)$$
$$\dot{\mu}^{\text{in}}_4 = \dot{\mu}^{\text{in}}_{\text{F}} \cdot \frac{\omega_{\text{F}}}{f_{\text{stoich}}\Phi} \quad (70)$$
$$\frac{f_{\text{stoich},2}}{f_{\text{stoich}}} j_1 + j_2 = \dot{\mu}^{\text{out}}_{\text{V}}\, \omega^{\text{V}}_{2,\text{e}} \quad (71)$$
$$\frac{f_{\text{stoich},3}}{f_{\text{stoich}}} j_1 = \dot{\mu}^{\text{out}}_{\text{V}}\, \omega^{\text{V}}_{3,\text{e}} \quad (72)$$
$$-\frac{1}{f_{\text{stoich}}} j_1 + \dot{\mu}^{\text{in}}_4 = \dot{\mu}^{\text{out}}_{\text{V}}\, \omega^{\text{V}}_{4,\text{e}} \quad (73)$$
$$\omega^{\text{V}}_{2,\text{e}} + \omega^{\text{V}}_{3,\text{e}} + \omega^{V}_{4,\text{e}} = 1 \quad (74)$$

where, at each iteration, the dimensionless vaporization rates j_i are given by

$$j_i = \frac{1}{N_{\text{F}}} \int\int -\dot{\mu}_i\, n\, d\mu\, d\omega \quad (75)$$

and the average mass fraction of EtOH in the chamber ($\overline{\omega}$) is given by Eq. 41.

The characteristic temperature scale associated with fuel combustion is determined by means of an order of magnitude analysis of the former energy balance (Eq. 63). To this end, we assume that all the fuel is vaporized and burned (i.e., $\dot{m}^{\text{out}}_{\text{S}} \simeq 0$, $I_1 + I_2 + \dot{m}^{\text{in}}_4 \simeq \dot{m}^{\text{in}}_{\text{F}}\left(1 + \omega_{\text{F}}/(f_{\text{stoich}}\,\Phi)\right)$) at the fuel feed wet-bulb temperature (i.e., $\dot{q}' \simeq 0$), and we also approximate the specific heats of all the vapors by a constant characteristic value $c_{\text{p,G}}$. Thus, we find the approximate value

$$T_{\text{e}} \simeq T_{\text{F}} + \frac{Q^{\text{in}}_{\text{F,eff}}/c_{\text{p,G}}}{1 + \frac{\omega_{\text{F}}}{f_{\text{stoich}}\Phi}} \quad (76)$$

leading us to define the dimensionless chamber temperature Θ_{e} as

$$\Theta_{\text{e}} \equiv \left(1 + \frac{\omega_{\text{F}}}{f_{\text{stoich}}\Phi}\right) \cdot \frac{T_{\text{e}} - T_{\text{F}}}{Q^{\text{in}}_{\text{F,eff}}/c_{\text{p,G}}} \quad (77)$$

Hence, in terms of the dimensionless chamber temperature Θ_{e}, the energy balance equation reads:

$$\int_0^{\Theta_e} \left(j_1 \frac{c_{\text{p},1}}{c_{\text{p,G}}} + j_2 \frac{c_{\text{p},2}}{c_{\text{p,G}}} + \dot{\mu}^{\text{in}}_4 \frac{c_{\text{p},4}}{c_{\text{p,G}}}\right) d\Theta = \left(1 + \frac{\omega_{\text{F}}}{f_{\text{stoich}}\Phi}\right) \cdot \left(\dot{\mu}^{\text{in}}_{\text{F}} - \dot{\mu}^{\text{out}}_{\text{S}} Q + q\right) \quad (78)$$

where we have defined the dimensionless variables Q and q as

$$Q \equiv \frac{Q^{\text{out}}_{\text{F,eff}}}{Q^{\text{in}}_{\text{F,eff}}}, \quad q \equiv \frac{t_{\text{ref}}\, \dot{q}'}{N_{\text{F}}\, m_{\text{ref}}\, Q^{\text{in}}_{\text{F,eff}}} \quad (79)$$

Note that while Q is of order 1, we expect that $q \ll 1$.

To solve the mass and energy balance equations in a numerically efficient way, at each iteration, we first solve the mass balance equations (Eqs. 68–74). Then, Q is updated according to the new value of $\overline{\omega}$ (recall that whereas $Q^{\text{in}}_{\text{F,eff}}$ is constant, $Q^{\text{out}}_{\text{F,eff}}$ depends on $\overline{\omega}$), and q is updated according to

$$q = \frac{1}{N_{\text{F}}} \int\int \left[-\frac{h_1[T_{\text{WB}}(\omega)] - L'_1}{Q^{\text{in}}_{\text{F,eff}}} \cdot \dot{\mu}_1 - \frac{h_2[T_{\text{WB}}(\omega)] - L'_2}{Q^{\text{in}}_{\text{F,eff}}} \cdot \dot{\mu}_2 - \frac{c^{\text{L}}_{\text{p,F}}\, T'_{\text{WB}}(\omega)}{Q^{\text{in}}_{\text{F,eff}}} \cdot \mu\, \dot{\omega}\right] n\, d\mu\, d\omega \quad (80)$$

with Θ_{e} fixed at the value corresponding to the former iteration. We use this approximation because $T_{\text{WB}}(\omega)$ is also a function of the chamber temperature, actually quite time-consuming to calculate (as it involves solving Eq. 6 with $dT_{\text{w}}/dt = 0$ for each particular couple of values of ω and T_{e}). Once this is done, Eq. 78 (with the LHS treated as a function of the unknown value Θ_{e}) is solved for Θ_{e} using Newton's method.

The former self-consistent population-balance and mass/energy-balance iterative process is repeated until 10^{-6} accuracy is reached for all quantities involved (chamber temperature and composition). Once this precision has been achieved, the relevant combustor performance indices combustion efficiency and combustion intensity are evaluated.

Combustor performance indices: quantities of interest and their relation to n(m, ω)

A principal objective of the present work is the calculation of interesting combustor performance indices, including the fractions of fuel and water actually vaporized ($f_{vap,1}$ and $f_{vap,2}$ respectively):

$$f_{vap,1} = \frac{I_1}{\dot{m}_F^{in}\omega_F}, \quad f_{vap,2} = \frac{I_2}{\dot{m}_F^{in}(1-\omega_F)} \tag{81}$$

as well as the total fraction of spray vaporized $f_{vap} = 1 - \dot{m}_S^{out}/\dot{m}_F^{in}$, given by

$$f_{vap} = \omega_F f_{vap,1} + (1-\omega_F) f_{vap,2} = \frac{I_1 + I_2}{\dot{m}_F^{in}} \tag{82}$$

Especially important are the corresponding combustion efficiency (η_{comb}) and combustion intensity[1] ($\mathcal{I}$). These last two parameters provide the most relevant overall picture of combustor performance, useful for making comparisons between different spray combustors (e.g., geometries, liquid fuels, operating conditions,…).

These combustion performance indices can be computed once the former self-consistent scheme has been implemented, and the corresponding steady-state spray population in the combustor $n(m, \omega)$ as well as the in and out mass flow rates and the chamber temperature, are known.

The combustion efficiency η_{comb} is the fraction of the effective fuel energy released in the combustor per unit time usable to produce thrust (or more generically: ''work''). If the ''fuel'' feed spray is un-diluted, and we assume that all fuel vaporized is burned (i.e., $f_{vap,1}\ \Phi \leq 1$), then η_{comb} is simply the fraction of fuel actually vaporized and burned in the chamber, $f_{vap,1}$. However, in our case, we must account for the fact that a fraction of the energy released by EtOH vapor combustion is used to vaporize the water carried in the diluted fuel feed spray. Making this correction, we find:

$$\eta_{comb} = f_{vap,1} \cdot \frac{\dot{m}_F^{in}\omega_F Q_{1,eff} - I_2 L_2}{\dot{m}_F^{in}\left[\omega_F Q_{1,eff} - (1-\omega_F)L_2\right]} \tag{83}$$

where the effective heat of combustion of the fuel $Q_{1,eff}$ takes into account the fraction of the heat used to vaporize the liquid fuel and the oxidizer (O_2(L))

$$Q_{1,eff} \equiv Q_1 - L_1 - \frac{L_{4,eff}}{f_{stoich}\Phi} \tag{84}$$

Recalling the definition of $Q_{F,eff}^{in}$ above, we find that the combustion efficiency is given by

$$\eta_{comb} = f_{vap,1} \cdot \left[1 + \left(1 - f_{vap,2}\right)\frac{(1-\omega_F)L_2}{Q_{F,eff}^{in}}\right] \tag{85}$$

Another relevant combustor performance index is the dimensionless combustion intensity ($\mathcal{I}$), defined here as the ratio of the chemical energy released in the combustor per unit time and per unit chamber volume ($\dot{q}_{chem} = I_1\ Q_1$), to the energy released per unit time and per unit volume associated with a Sauter-mean-diameter (d_{32}) feed droplet (given by $\rho^L\ \omega_F\ Q_1/t_{vap}$). Recalling our former definitions as well as the mass and energy balances (see previous section), we find that $\mathcal{I}$ is given by

$$\mathcal{I} = \frac{\rho_{ch}/\rho_L}{Dam} \cdot \frac{f_{stoich}\Phi/\omega_F}{1 + f_{vap}f_{stoich}\Phi/\omega_F} \cdot f_{vap,1} \tag{86}$$

where ρ_{ch} is the density of the gases in the chamber corresponding to the far-field, self-consistent, ambient conditions, and ρ_L is the density of the liquid spray feed.

This completes our present theoretical model of bivariate fuel spray combustion—anticipating a class of applications in which the fuel is a concentrated solution of EtOH in water, and the oxidizer is vaporized O_2(L). In the following section, we present a series of results concerning, first, the behavior of individual droplets under prescribed chamber conditions, then the solution of the PBE under prescribed chamber conditions, and, finally, results corresponding to the fully coupled (fuel spray + spray-dependent chamber conditions), computed according to the former iterative scheme—in which case, we also show results for the two aforementioned combustor performance indices: efficiency and intensity.

Illustrative Quantitative Results: Von Braun's V-2 Liquid Propellant Rocket Motor

Behavior of individual droplets: departures from d^2-law; preferential ethanol loss, temperature "history"

This section contains results for the time-evolution of individual droplets under constant (reference) ambient conditions. In the numerical computations shown below, the reference far-field gas composition, temperature, chamber pressure, and initial droplet composition correspond to the V-2 rocket and are given in Table 1. Results shown below have been computed solving numerically Eqs. 9–11. The initial droplet size considered is $d_{32} = 30\ \mu$m, the initial droplet temperature is T_{WB} corresponding to an initial droplet composition $\omega(0) = \omega_F = 0.75$ and the aforementioned reference ambient temperature and composition.

Results for droplet mass and composition are shown in Figures 1 and 2. Note that EtOH vaporizes much faster than water (as expected), so that the droplet composition becomes almost pure water at $\tau \sim 0.75\ \tau_{vap}$. This figure also shows that the rate of water vaporization increases after the EtOH is essentially completely vaporized. This is because T_{WB} for pure water is higher than that for water containing a significant amount of EtOH.

The time history of droplet temperature is shown in Figure 3, where we can see that the droplet temperature remains extremely close to T_{WB} at all times (slightly below the mixture boiling temperature θ_b). In particular, at $\tau \sim 0.75\ \tau_{vap}$, the amount of EtOH in the droplet essentially vanishes and, as mentioned above, T_{WB} increases sharply, leading to the observed behavior of θ/θ_{WB} shown in Figures 3 (right) and 4 (right). Note that even during this short transient (in which the droplet temperature must adapt to the new T_{WB}), the difference between T_w and the T_{WB} is negligible.

Finally, Figure 4 shows results for the individual droplet rate laws as a function of time during the vaporization process. In this figure, we see that, during the first part of the process ($\tau < 0.75\ \tau_{vap}$) $\dot{m}_1$ decreases nearly linearly with

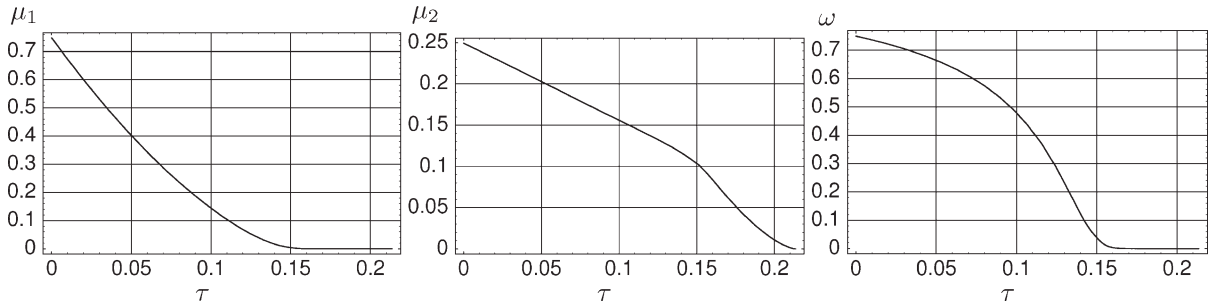

Figure 1. Dimensionless presentation of individual fuel droplet mass and composition vs. time: μ_1 (left), μ_2 (center), ω (right).

time, whereas $\dot{m}_2$ has a (relatively small) constant value, and $\dot{T}$ is slightly positive (as the water content of the droplet increases). At the moment of almost complete EtOH vaporization, T_{WB} increases sharply, and the droplet experiences a short interval characterized by transient heating and an increase in water vaporization rate. After this transient, during the last part of the process ($\tau > 0.75\ \tau_{vap}$) $\dot{m}_1$ is essentially zero while $\dot{m}_2$ decreases nearly linearly with time and $\dot{T}$ is almost zero. The qualitative difference between the first and the last part of the process can also be appreciated very clearly in Figure 2 (right), where we see that the mass transfer driving force (B_m) has two different (and almost constant) values, depending on whether the EtOH content of the droplet is (or is not) negligible.

Summarizing, we may say that EtOH + water droplets vaporize in a sequential way, with a short transient between the EtOH vaporization period and the water vaporization period. On the other hand, our results show that if the initial droplet temperature is equal to the size-insensitive wet-bulb temperature T_{WB}, then it remains very close to the time-dependent T_{WB} throughout the entire binary-system vaporization process.

PBE-results under specified (reference-) chamber conditions

The mathematical method used to solve the PBE governing the steady-state bivariate droplet population in the combustion chamber is first illustrated in the present section, where PBE-solutions corresponding to constant (reference) chamber conditions are presented. This same mathematical scheme will also be used to solve the PBE in the fully coupled problem (next section) where the chamber conditions are computed (in an iterative, self-consistent fashion) based on the solution found for the steady-state bivariate droplet population.

Although a formal analytical solution for the bivariate NDDF n has been provided (see Eq. 34), evaluation of this NDDF requires numerical integrations containing the functions $A(\omega)$ and $B(\omega)$. Each numerical evaluation of these functions is quite time consuming, because it requires solving a nonlinear equation for the droplet wet-bulb temperature as well as computing the corresponding gas-phase mass fractions at the droplet surface by means of the VLE condition.

As our goal is to iteratively solve the fully coupled problem (steady-state spray + combustion chamber), we need an efficient method to solve the PBE, because we must solve this equation many times in any self-consistent iterative scheme. Consequently, we need an efficient method to evaluate the functions $A(\omega)$ and $B(\omega)$, (the principal time-consuming task needed to solve the PBE). To this end, $A(\omega)$ and $B(\omega)$ were approximated by means of an Orthogonal-Collocation expansion in terms of Chebyshev polynomials using Gauss-Lobatto abscissae in the interval $\omega \in [0, \omega_F]$. Use of Gauss-Lobatto abscissae is motivated by the requirements of high accuracy in both limits of the variable ω. In particular, for Damköhler numbers of order $\mathcal{O}(1)$ (or larger), n becomes a very highly peaked function of ω, located in the lower limit ($\omega \to 0$); whereas for very small values of the Damköhler number n is a peaked function of ω located close to the feed composition (ω_F). Thus, only when both limits of the interval are included in the set of abscissae used in the expansion, does it become possible to achieve high-accuracy results.

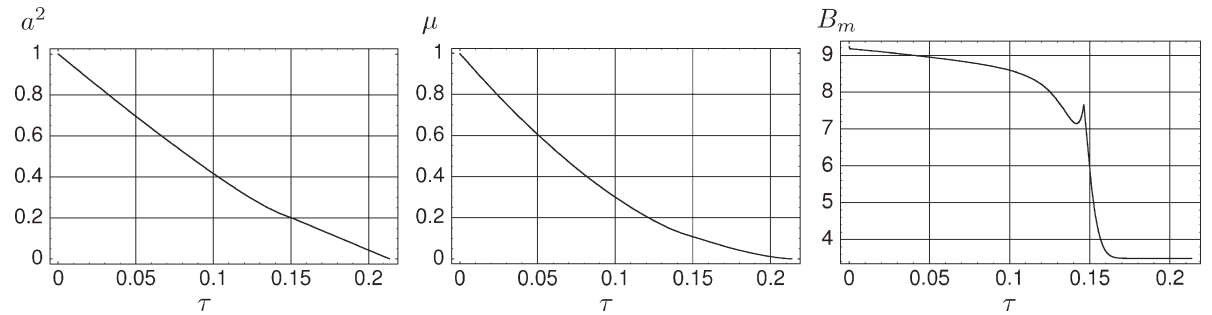

Figure 2. Dimensionless presentation of individual fuel droplet radius squared, mass, and mass-transfer driving force vs. time: a^2 (left), μ (center), B_m (right).

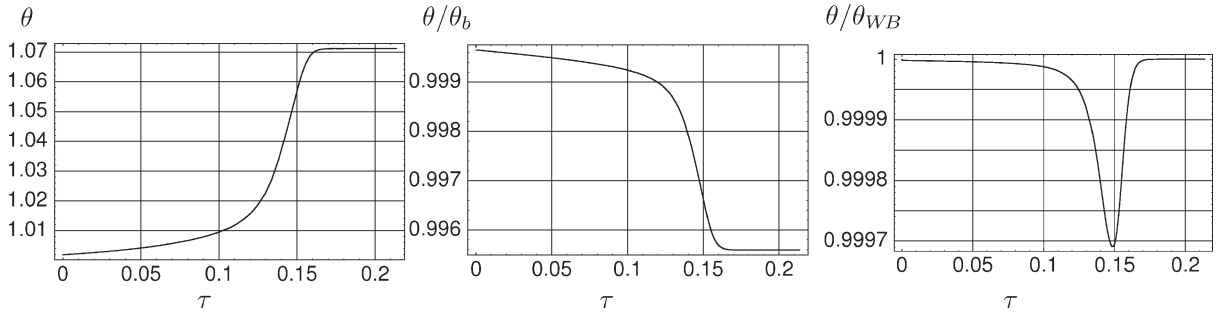

Figure 3. Dimensionless presentations of individual fuel droplet temperature vs. time: θ (left), θ/θ_b (center), θ/θ_{WB} (right).

The number of spectral components needed in the expansion of $A(\omega)$ and $B(\omega)$ was determined based on a convergence analysis for the function n and its moments for $\sigma_G = 2.3$, $Dam = 1$, and constant (reference) chamber conditions (Table 1). The reason for this choice is because the case $Dam = 1$ leads already to a strongly peaked n at ω close to 0, which does not change much as higher vaporization Damköhler numbers are considered. On the other hand, convergence rate had only a mild dependence on the feed spread parameter σ_G (in the range $1.7 \leq \sigma_G \leq 2.3$), with the lowest convergence rate corresponding to the highest feed spread. As a consequence, we believe that convergence for this particular choice of parameters ensures similar accuracy for other values of the parameters in the range of physical interest. The convergence criterion finally adopted was to have at least 6 digit accuracy for all the lowest order moments of n: $\langle \mu^k \omega^l \rangle$, with $k, l = 0, 1, 2$.

As a consequence of the model used for the reference Fick diffusion coefficient (D_{ref}), which involves absolute values of $\omega_{i,w} - \omega_{i,e}$, the functions $A(\omega)$ and $B(\omega)$ have a discontinuity in the first derivative. Because of this behavior, a relatively large number of spectral components (ca. 30) was needed to achieve high accuracy convergence. The functions A and B, have been finally computed using 50 Gauss-Lobatto spectral components, producing an extremely accurate approximation which, at the same time, is very fast to evaluate.

As an illustration of the results found using this numerical strategy, we show in Figure 5 the steady-state NDDF [$\mu\, n(\ln \mu,\omega)$ vs. $\ln \mu$ and ω] corresponding to the aforementioned reference chamber conditions (Table 1). The surface shown in Figure 5 has been actually drawn as a 3-D parametric plot of several characteristic paths, for values of ω between ω_F and 0, corresponding to initial values of $\ln \mu$ between -10 and 10. Each one of these characteristic paths departs from the "boundary" condition Eq. 21, as also shown in Figure 5.

Note that the number density function is bi-modal with respect to ω. The reason for this is clear, on one hand, the feed spray has the highest possible value of $\omega = \omega_F$, whereas all the droplets leave the domain of integration at the lowest possible value $\omega \to 0$. The qualitative shape of this NDDF, computed under prescribed chamber conditions, also applies to self-consistent results computed using the iterative scheme presented bellow (see Figure 9).

Self-consistent results for the PBE

The self-consistent scheme based on mass/energy balances outlined in the previous section was used to calculate chamber conditions corresponding to steady-state operation of the V-2 rocket. Convergence of the scheme is quite fast, with a tolerance of 10^{-6} about 7–10 iterations were needed for reference vaporization Damköhler numbers larger than 0.1, whereas a number of iterations between 10 and 40 were needed for smaller reference Damköhler numbers, down to 0.04. The computation time needed for each iteration on a modern PC was about 35s, yielding a total computation time of about 1.5h for all cases shown.

Results corresponding to V-2 rocket, obtained with the former self-consistent scheme, are shown in Figures 6–8 as a function of the vaporization Damköhler number Dam_{vap}, defined as the ratio of the characteristic residence time to the vaporization time for a droplet of Sauter-mean diameter, under converged (self-consistent) chamber conditions. In this respect, recall that the vaporization Damköhler number ($Dam = Dam_{ref}$) that enters the PBE is a "reference" value, defined using the characteristic vaporization time-scale under

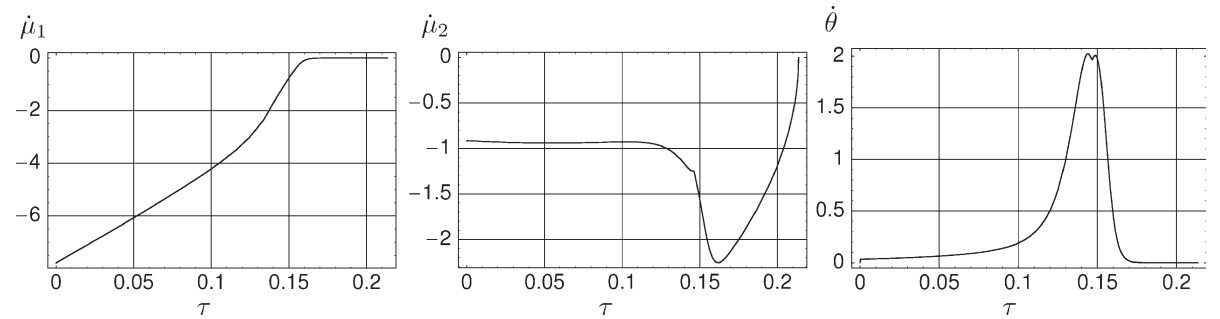

Figure 4. Dimensionless presentation of individual fuel droplet rate laws vs. time: $\dot{\mu}_1$(left), $\dot{\mu}_2$(center), $\dot{\theta}$(right).

reference environment conditions. Once the self consistent scheme has converged and the steady-state chamber conditions are known, the actual vaporization Damköhler number (Dam_{vap}) can be computed using

$$Dam_{\mathrm{vap}} = Dam_{\mathrm{ref}} / \tau_{\mathrm{vap,\ QS,\ } d_{32}} \tag{87}$$

where $\tau_{\mathrm{vap,\ QS,\ } d_{32}}$ is the dimensionless vaporization time of a droplet with Sauter-mean diameter under steady environment conditions derived from the self-consistent calculation. Our results for Dam_{vap} vs. Dam_{ref} are shown in Figure 6. Although all calculations were performed as a function of the reference vaporization Damköhler number, these performance results are shown as a function of the more physically meaningful Dam_{vap}.

Results for the steady-state, self-consistent, ambient chamber conditions (composition and temperature) are shown in Figure 7 [It was observed that the correction q (Eq. 80) in the energy balance equation (Eq. 78) is, indeed, negligible (less than 0.5%)].

As an indication of the performance characteristics of the V-2 rocket thrust chamber, the combustion efficiency η_{comb} (Eq. 85) and intensity $\mathcal{I}$ (Eq. 86) are shown in Figure 8. The calculation of these two indices was performed once the aforementioned self-consistent scheme had converged.

Finally in Figure 9, we show the self-consistent steady-state droplet distribution functions corresponding to 3 values of the (reference) vaporization Damköhler number as a function of droplet state variables: mass and composition (Figure 9 top). These results are also presented as a 3-D parametric plot of a collection of representative characteristic lines that depart from the ''boundary'' condition for n, also shown.

Although the results presented here have been computed using droplet mass and composition as the independent variables (for reasons already explained), an interesting result of the present model is the possibility of visualizing these

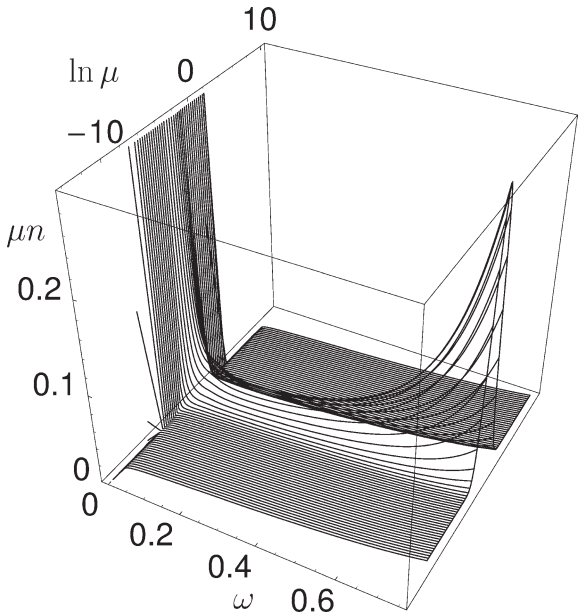

Figure 5. Steady-state mass-weighted number density distribution function: $\mu\, n(\mu, \omega)$ vs. ($\ln \mu$, ω) corresponding to $Dam_{\mathrm{vap}} = 1$ under prescribed (constant) chamber conditions (Table 1).

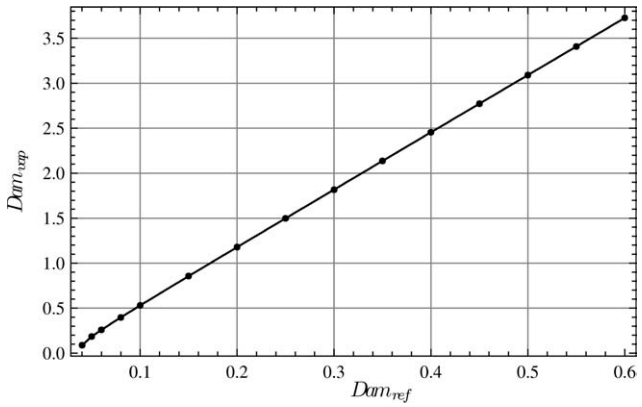

Figure 6. Fuel droplet vaporization Damköhler number vs. reference vaporization Damköhler number.

NDDFs as a function of any other set of droplet state variables. For instance, in Figure 9 bottom, we present the corresponding NDDFs as a function of dimensionless droplet diameter ($d_{\mathrm{p}} = 2R/d_{32}$) and T_{WB}. Although this pair of state variables would not be a good choice for carrying the numerical computations, the steady-state NDDF in terms of these state variables may now be measurable by optical methods, possibly facilitating future comparison of such numerical results with actual experimental results.

Discussion: Defense of Assumptions, Implications of Results, and Applications

"Condensation-induced boiling" (CIB) and its avoidance

Earlier in this research, we discovered/reported (Rosner and Arias-Zugasti)[10] the possibility/consequences of $\dot{m}_2$ being positive (H_2O uptake) for sufficiently high combinations of EtOH mass fraction in the feed droplet and water vapor concentration in the high-temperature combustion chamber. The heat-release rate associated with such water vapor condensation generally increases the droplet QS wet-bulb temperature but our overall isobaric diffusion-controlled vaporization rate approach is no longer self-consistent if T_{WB} reaches the corresponding equilibrium bubble point temperature of the vaporizing droplet at the prevailing total pressure. We labeled this interesting ''threshold'' condition, which has apparently escaped the notice it deserves, the ''condensation-induced-boiling'' (CIB-) locus, and immediately estimated its location (on the $\omega_{2,\mathrm{e}}$ vs. ω_1^{L} plane) for both the German V-2 and derivative Russian RD-101 liquid propellant rocket motors. We are now in a position to ''refine'' these previous CIB-locus estimates, allowing for the full[†] mass- and energy-transfer rate coupling between the bivariate fuel droplet population and the self-consistent vapor phase ($\omega_{i,\mathrm{e}}$, T_{e}) in the chamber.

[†]Of course, our basic mathematical model (second section) presently incorporates deliberate simplifications readily relaxed in our future bio-fuel combustion calculations. Here, we merely mention two in this category: (1) Our approximate inclusion of liquid phase solution nonideality via the use of temperature-insensitive nonunity activity coefficients inferred from available $p = 1$ atm azeotrope data at 351.45 K. We are currently exploring and will ultimately introduce a rational way to estimate T-dependent EtOH and H_2O activity coefficients much above 400 K. (2) Our explicit neglect of combustion product dissociation—i.e., our current ''exclusion'' of such vapor species as: OH(g), H(g), O(g), etc., whose presence will inevitably correspond to systematic reductions in both predicted combustion gas temperature and mean molecular weight. Even when the oxidizer is O_2(g) rather than air, dissociation will be suppressed at high enough pressures.

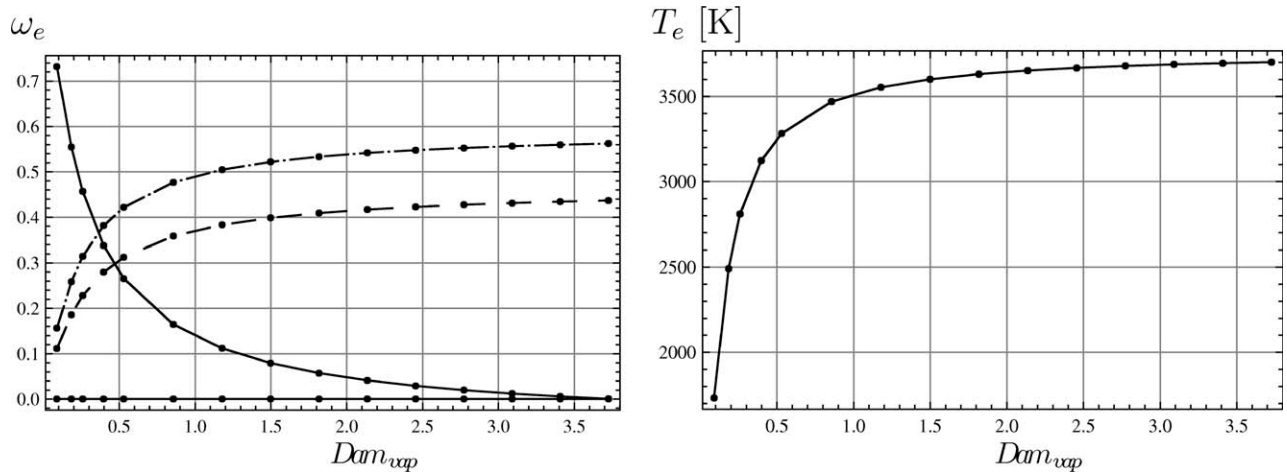

Figure 7. Model-predicted steady-state chamber composition (left) and absolute temperature in Kelvins (right) vs. fuel vaporization Damköhler number.

Composition shown: far-field mass fractions of ethanol (zero), oxidizer (which reaches a value very close to zero for $Dam_{vap} = 3.73$), H_2O (0.44 for $Dam_{vap} = 3.73$) and CO_2 (0.56 for $Dam_{vap} = 3.73$).

"Condensation-induced droplet boiling" imposes an interesting limitation on the "allowable" EtOH content of the fuel for "ordinary" steady-state adiabatic operation. Our present calculations reveal that V-2 operating conditions (with $\omega_1^L = 0.75$, Φ near 1.1, and $p = 15$ atm) were quite close to the previously estimated CIB-locus (see Figure 1 of Ref. 10). An intriguing corollary of this finding is that the purpose of 25 wt % water in the V-2 thrust chamber fuel may not have been exclusively to improve its regenerative (and "film-") coolant properties (see also, Rosner and Arias-Zugasti)[10].

Does the unconditional spray size distribution remain log-normal?

Although we have deliberately avoided imposing such assumptions, some approximate methods for rapidly solving population balance problems exploit the presumption that the "shape" of the continuous DSD remains approximately invariant—e.g., log-normal (see, for example, Vemury and Pratsinis,[11] Rosner and Tassopoulos,[12] and Bensberg et al.[13]) In this case, this would amount to the assumption that the exit DSD is also log-normal, albeit with a reduced geometric mean volume and perhaps, altered spread parameter. As the evaporation rate laws governing binary droplet diffusion-controlled evaporation are not as simple as ordinary "power-laws," we should not expect to "preserve" log-normality. On the other hand are such departures likely to be appreciable?

For these reasons, an interesting modeling question, which we are now in a position to answer, is: If the feed DSD is log-normal how "distorted" is the unconditional DSD of the surviving droplets (emerging from the combustion chamber)? In each case, these unconditional DSDs can be calculated from our characteristics-computed NDDFs because: (1) we know how the droplet mass density depends on both ω_1 and T, and (2) recall that $T = T_{WB}(\omega_1; p)$.

There are several ways to quantify DSD-"non-lognormality." Qualitatively, one can, say, compare the dimensionless distribution function $\langle v\rangle n(v)/N_p$ vs. $v/\langle v\rangle$ on semi-log

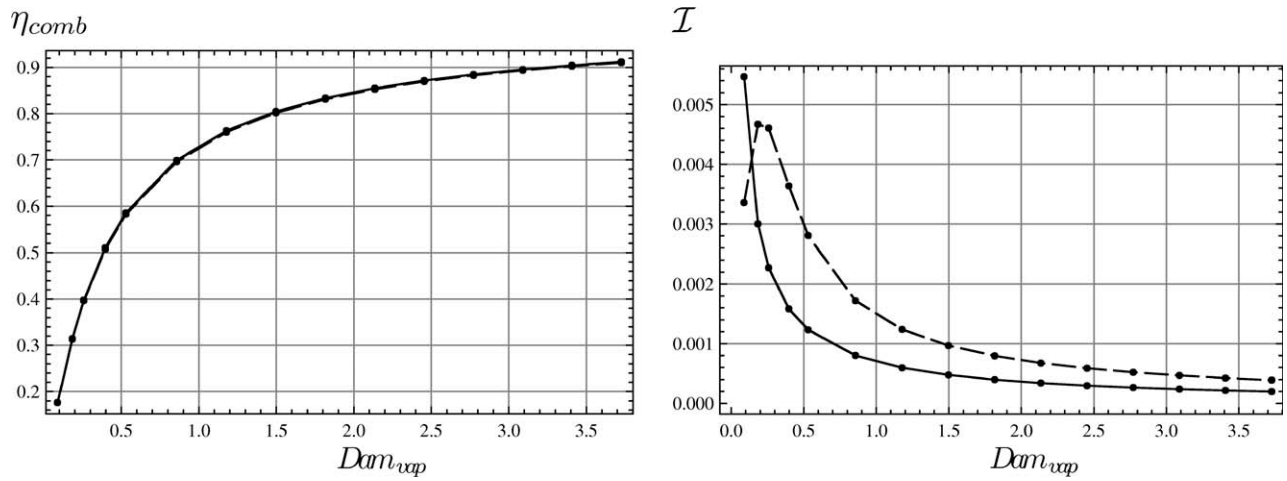

Figure 8. Combustion efficiency (left) and dimensionless combustion intensity (right) vs. fuel vaporization Damköhler number (Solid curve corresponds to present bivariate spray model, broken curves correspond to "pseudo-unary" approximation[1]).

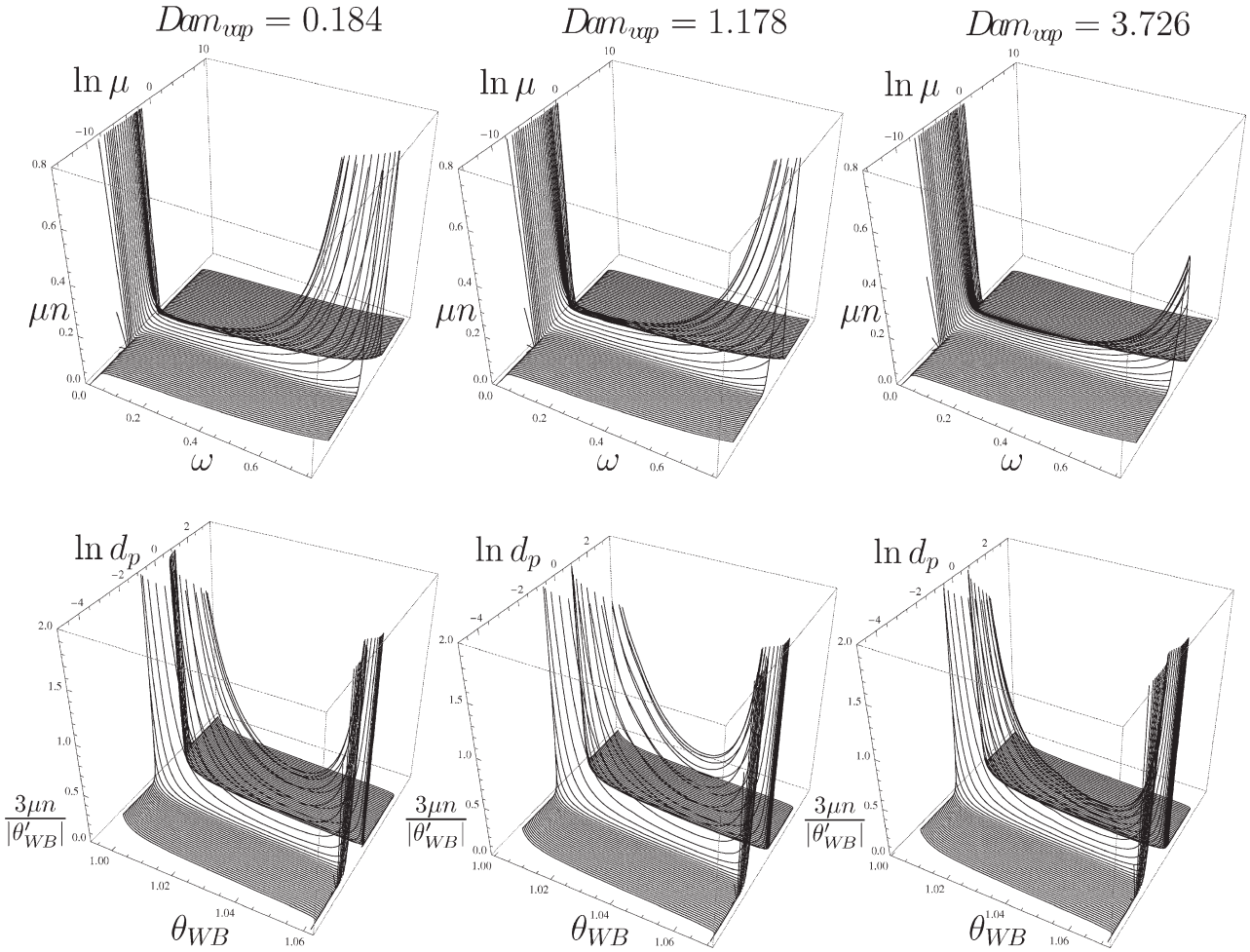

Figure 9. Self-consistent steady-state number density (joint-) distribution functions corresponding to Dam_{vap} = 0.184 (left), 1.178 (center), and 3.726 (right) as function of dimensionless droplet mass and composition (top) or dimensionless droplet diameter and wet-bulb temperature (bottom).

coordinates, and look for non-Gaussian features, if not multiple modes. In this case, we have chosen to demonstrate non-log-normal behavior by examining the normalized dimensionless lowest order moments of the unconditional DSD function in terms of droplet mass $\langle \mu^k \rangle / \langle \mu \rangle^k$ (computed using Eq. 39, with $\alpha = k$ between 0 and 6, and $\beta = 0$), as compared with the corresponding moments of the log-normal distribution fitted to reproduce the first three moments ($\langle \mu^k \rangle$ with $k = 0, 1, 2$). Results are shown in Figure 10, where the natural logarithm of these moments has been plotted for several vaporization Damköhler numbers. The results shown in Figure 10 are based on the (self-consistent, QS) DSDs shown in Figure 9. Recalling that the feed unconditional DSD in terms of droplet mass considered in the present calculations is log-normal, it is natural to expect that the computed self-consistent steady-state DSD in the combustion chamber must remain near-log-normal in the limit of low vaporization Damköhler numbers. This is indeed observed in Figure 10. On the other hand, Figure 10 shows that the difference between the real DSDs and their corresponding log-normal best-fits increases very rapidly with the vaporization Damköhler number, as expected. Actually, even for Dam_{vap} as low as 0.20 the relative error in the third normalized dimensionless moment (related to the symmetry of the NDDF) is already higher than 17%, and, of course, this error increases very rapidly with moment index as well as with Dam_{vap}.

In summary, the present idealized analysis shows that, even if the feed DSD is log-normal for droplet mass, the steady-state DSD in/exiting from the combustion chamber is not log-normal. Significant differences between the real DSD in the combustion chamber and the log-normal best fit should be expected for Dam_{vap}-values of order unity or higher.

Possibility of a "pseudo-unary" approximation?

In this work, emphasizing performance of the liquid "biofuel" EtOH, we have emphasized the true bivariate nature of such spray combustors. However, because these generalizations of our earlier univariate analysis (Rosner et al.[1]) clearly increase the mathematical and numerical complexity of the problem, it is natural to inquire if some "pseudo-unary" representation of such a fuel could lead to reasonable performance estimates with much less computational effort and shorter "turn-around" times. This possibility can now be investigated using our present "numerically exact" bivariate

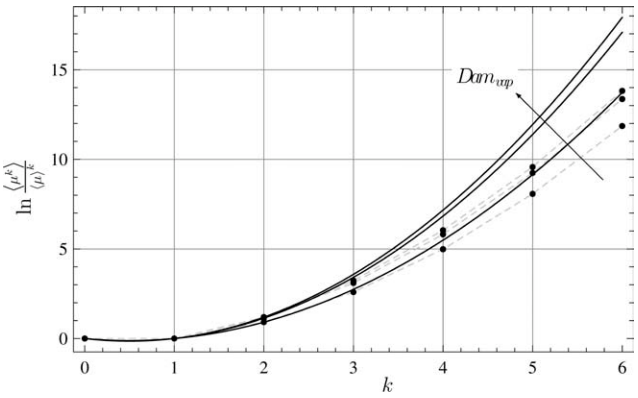

Figure 10. Momens of the unconditional, self-consistent, steady-state droplet size distributions in terms of droplet mass (dots joined by straight dashed lines), compared with the moments of the corresponding size distributions fitted to a log-normal distribution (solid lines); for Dam_{vap} = 0.184, 1.178, and 3.726.

results. For brevity, we limit ourselves here to only one such example, explored for the "base case": feed $\Phi = 1.1$, $p =$ 15 atm, $\omega_1^L = 0.75$, feed $d_{32} = 30$ μm, $\sigma_G = 2$. Imagining that this fuel behaves like a single substance with the "effective" heat of vaporization: $L_{\text{eff}} = \omega_1^{\text{L}} L_1 + (1 - \omega_1^{\text{L}}) L_2$, etc. and neglecting the actual tendency for such droplets to change their composition during their vaporization lifetimes, we can formally make idealized spray combustor efficiency and intensity predictions using the methods of Rosner et al.[1] The (limited) "success" of this type of approximate method when applied to the V-2 test problem is demonstrated in Figure 8, where these two indices are shown as a function of the vaporization Damköhler number. As can be seen, as the best possible "pseudo-unary"[1] approximation (fitted to have the correct overall heat of combustion and Dam_{vap}) is able to predict the fraction vaporized to within ca. 5% (Figure 8, left), it fails to provide a reasonable prediction for the combustion intensity (Figure 8, right) irrespective of the magnitude of the vaporization Damköhler number.

We conclude that the "pseudo-unary" approximation, often used in spray combustion modelling, fails to accurately predict the (volumetric chemical energy release) performance of composition-varying fuels, as in the case of the EtOH-based fuel-fired spray combustors considered here. Similar results can be expected for other liquid fuels, comprised of fully miscible blends of many liquid components with different volatilities. In such cases, a "continuous mixture" approach can provide an accurate approximation at reasonable computational cost.[12,14]

Defense of present approximations

Many of the assumptions underlying our present idealized spray combustor model (i.e., well-("jet-)stirred reactor," droplet vaporization-controlled chemical energy release rate, continuous, adiabatic,…) were already itemized and defended in Rosner et al. [1] For this reason, we focus here on those assumptions important to our present generalizations to capture the behavior of two-component fuel droplets—here EtOH + H_2O—where the components are fully miscible but have unequal volatility and form noticeably nonideal liquid solutions (Rosner and Arias-Zugasti[10]). Recalling relevant portions of our second section above, these particular assumptions can be identified as: (A1) QS vapor phase diffusion-controlled fuel droplet evaporation rates; (A2) each droplet remains internally well-mixed throughout its evaporative lifetime; (A3) local VLE exists throughout its evaporative lifetime. Of course, each of these assumptions has been introduced because it enables the simple quantitative treatment of an otherwise more complex situation. In this class of applications, these simplifications are, mercifully, justifiable, for the reasons stated below.

Taking these in turn:

A1. As discussed in Ref. 1, the dimensionless parameter governing departures from the QS-approximation can be written in terms of the prevailing mass density ratio and driving force parameter B_{m} (see Eq. 3 of Ref. 1); i.e.,

$$\varepsilon \equiv \left(\frac{2}{\pi} \cdot \frac{\rho_{\text{G}}}{\rho_{\text{L}}} \cdot \ln(1 + B_{\text{m}}) \right)^{1/2} \tag{88}$$

and ε becomes non-negligible when the chamber pressure is high enough to be "trans-critical." In the class of applications, we are considering chamber pressures were near ("only") 15 atm, whereas the "pseudo-critical" pressure for, say, 75 wt % EtOH, 25 wt % H_2O is as high as ca. 63 atm. Indeed, we estimate that the parameter ε never exceeds about 0.07 for our base case—corresponding to non-QS effects on isolated unary droplet evaporative lifetimes in a constant vapor environment less than about 7 pct. On this basis, our exploitation of the QS-approximation to provide convenient rate laws for $\dot{m}_1$ and $\dot{m}_2$ appearing in the bivariate PBE (Eq. 16) is considered reasonable.

A2. Although the molecular thermal conductivity ratio k(gas)/k(L) is small enough so that each fuel droplet may be considered nearly isothermal at any instant, it is likely that our internally well-mixed approximation tends to systematically over estimate the EtOH mole fraction x_1 at $r = R(t)$ and, hence, systematically under estimate the complementary H_2O mole fraction there.

In the absence of appreciable internal circulation, the dimensionless Peclet group governing internal (liquid phase) mass diffusion limitations can be written:

$$Pe_{\text{m}}^{\text{L}} = \frac{R\left|\dot{R}\right|}{D_{12(\text{L}),\text{ref}}} \tag{89}$$

where $R(t)$ is the droplet radius, $D_{12(\text{L}),\text{ref}}$ is an appropriate liquid-phase molecular binary Fick diffusivity. For QS diffusion-controlled evaporation (see A1 above), this can be shown to be equivalent to the size-independent and (explicitly) pressure-insensitive product of a large and small number, i.e,:

$$Pe_{\text{m}}^{\text{L}} = \frac{D_{1-\text{mix}(\text{G}),\text{ref}}}{D_{12(\text{L}),\text{ref}}} \cdot \frac{\pi}{2} \varepsilon^2 \tag{90}$$

where ε is the aforementioned non-QS parameter. Inserting, a $D_{12,\text{ref(L)}}$-value near 2×10^{-8} m^2/s, under V-2-like conditions Pe_{m}^{L} seems to be of $\mathcal{O}(1)$, despite the smallness of ε.

On this preliminary basis such droplets would not be molecularly "well-mixed"—justifying future attention to relaxing this particular assumption. For the present, however, we note that the numerical value of $D_{12(L),ref}$ is itself rather uncertain, and in practice there may be sources of convection within droplets that facilitate the internal mixing process [indeed, under actual propulsion conditions the limit we consider may be more realistic than the opposite (less tractable) limit of exclusively radial liquid phase molecular diffusion]. In any case, given our overall objectives, these facts, combined with the computational simplicity of the internally well-mixed limiting case, explain the modeling choice made here.

A3. For our present engineering calculations, considering nonequilibrium QS-state droplet evaporation (here with a net mass flux and non-zero Fourier energy flux) is not actually incompatible with our present approximation of local VLE at the vapor/liquid interface. In effect, we are simply neglecting the interfacial resistances to mass and energy transfer compared with those in the moderately dense adjacent vapor phase (see, e.g., Rosner and Papadopoulos[15]). This is the usual situation for physical as opposed to chemical interfacial transformations, especially when the vapor molecular mean-free path is extremely small on the scale of the vapor-phase diffusion boundary layer thicknesses. This follows from the fact that molecular evaporation coefficients in such chemically simple liquids are not likely to be much smaller than $\mathcal{O}(1)$.[16]

One remaining assumption underlying our V-2 illustrative calculations is also noteworthy. Although we have here focused on the evaporation rate of the fuel droplets, the V-2 spray combustor was actually a "bi-propellant" system—meaning that both the oxidizer [here $O_2(L)$] and fuel entered the combustion chamber as liquids. In effect, we have therefore assumed that $t_{vap,O_2(L)} \ll t_{vap,F}$, where the "Fuel" is (here) EtOH (+ 25 wt pct H_2O)—i.e., we have assumed rapid $O_2(L)$ droplet evaporation. Put another way, $O_2(g)$ "availability" for EtOH vapor phase combustion was not considered to be a performance-limiting rate process.

At first glance, this seems "plausible" (because the latent heat of fuel vaporization, L_F is about 5.6 times that of $L_{O_2(L)}$), but the fact that it is the $\ln(1 + B_m)$-ratio that "counts" (see, Eq. 88) leads to the (somewhat surprising) result that, if $d_{32O_2(L)}$ were actually equal to d_{32F}, the $O_2(L)$/F t_{vap}-ratio would be as large as about 0.6 under such conditions.

However, it is possible to defend this particular assumption because a comparison of the remaining physical properties (liquid surface tension, viscosity, and density) of $O_2(L)$ and this fuel suggests that $d^2_{32O_2(L)}$ will be much smaller than d^2_{32F}—probably enough to make the aforementioned t_{vap}-disparity at least first order-of-magnitude. This can be quantified using what is known about pressure-driven "atomizer" performance, conveniently reviewed by Lefebvre.[17,18] For example, one cited correlation (attributed to El Kotb (1982)) indicates that: $d_{32} \sim (\mu_L/\rho_L)^{0.385} \cdot (\rho_L\gamma_L)^{0.737}$. We estimate that the surface tension of this fuel is higher than that of $O_2(L)$ by a factor of about 2.1 (at their respective injection temperatures) and the viscosity is probably higher by a factor of 4.2, whereas, as is better known, the fuel density is lower than that of $O_2(L)$ by the factor of only about 1.3-fold. Combining these ratios and power-law dependencies leads to the conclusion that (for comparable injector pressure drops and hole sizes) d_{32F} will be larger than $d_{32_{O_2(L)}}$ by a factor of about 2.8. Therefore, if both evaporation rate processes are vapor phase (heat) diffusion-controlled, the characteristic oxidizer droplet vaporization lifetime will be smaller than that of the fuel by somewhat more than one decade. However, as beyond the scope of our present work, these estimates suggest that future attention will have to be directed to the performance consequences of non-disparate vaporization times in bipropellant liquid systems—as in the case of, say, hydrazine/nitrogen tetroxide.

Conclusions and Broader Engineering Implications

In this work, the steady-state, bivariate NDDF for fuel droplets (comprised of EtOH containing H_2O, assumed internally well-mixed) in the combustion chamber of a particular class of idealized high-pressure spray combustors (the V-2 liquid propellant rocket motor) has been computed, probably for the first time. Our mathematical method is based on solving the corresponding population-balance PDE using the method-of-characteristics, together with overall mass and energy balances that relate the chamber gas temperature and composition to the amount of fuel vaporized and burned.

Although our mathematical model is based on important idealizations, the methods used are self-consistent, and enable the extremely efficient/accurate calculations of important overall combustion performance indices, such as combustion efficiency (relative amount of fuel vaporized and burned) and combustion intensity (volumetric chemical energy release rate), as functions of the combustor control parameters (i.e., droplet vaporization-based Damköhler number (analyzed in detail here), or chamber pressure, feed fuel droplet size (and/or composition) distribution function, fuel-substitution, etc.).

Our illustrative results show that to accurately predict the vaporization rate-controlled combustion intensity for spray combustors using composition-varying fuels (e.g., even liquid EtOH, considered here), it is necessary to introduce state variables that transcend droplet size. Our results also show that the common approximation of an invariant "presumed-mathematical-form" for the droplet NDDF leads to errors that increase rapidly with the vaporization Damköhler number, becoming unacceptable at Damköhler numbers associated with acceptable efficiency levels.

We believe that this class of population-balance-based mathematical models will be useful to (1) set instructive bounds on the achievable steady-state performance of "real" spray combustors, (2) economically map out the sensitivity of spray combustor performance to a large number of important control parameters, and, perhaps most important, (3) guide the development of future "sufficiently comprehensive" mathematical models to facilitate the future development of this interesting class of multiphase chemical reactors.[2]

Principal conclusions of present study

We expect qualitatively similar behavior for the case of the "sister"-fuel: methanol (MeOH) + H_2O, not explicitly studied here. In other applications, partial "fuel substitution" may be motivated by the opportunity to "incinerate" a solvent (like impure benzene) perhaps uneconomical to recover,

but readily dissolved in the primary liquid fuel (e.g., kerosene-like) fed to an incinerator. In this connection, we also note that biofuel synthesis and downstream processing often produce a mixture of isomers—e.g., several butanols, along with inevitable impurities (e.g., acetone,…)

Although there appears to be no conceptual or procedural obstacles to using our present characteristics-based numerical scheme to treat combustors fired with sprays containing 3, 4, 5,… species, when this number becomes impractically large, resort can be made to a rational choice of fewer "pseudo-species" using the methods of continuous mixture thermodynamics/transport (see, e.g., Rosner et al.[19] and Arias-Zugasti and Rosner[14]).

Present mathematical model as a convenient "test-bed" for the economical examination of conjectured simplifying approximations (pseudo-unary, internal-diffusion, bivariate QMOM,...)

As illustrated in the former section, our bivariate mathematical model of EtOH spray combustors can serve as a convenient "test-bed" for the economical examination of conjectured, often plausible, simplifying approximations. There we briefly examined the success of a univariate ("pseudo-unary") QS-representation of the present situation—as was found to be appropriate for the spray combustion of, say, dodecane-like fuel in a combustor chamber at pressure levels not much greater than 10 atm (or ca. 1 MPa).

Another simplification exploited in this work is that of the "internally well-mixed" droplet—i.e., neglect of intra-droplet mass-transfer limitations. Although the nature/success of this approximation has been studied for a single multi component droplet (see, e.g., Landis and Mills[20] and Shaw et al.[21]), to our knowledge, there are no definitive studies of the effect of this particular simplification for actual spray devices fed with a distribution of droplet sizes. We view this as but one of several attractive opportunities for future research (see former sub-section) because the present framework already provides one of the two important limiting cases (in terms of a Peclet number based on droplet surface recession velocity, droplet radius, and liquid phase Fick diffusion coefficient).

In short, we believe this strategy to be a cost-effective route to more faithful spray combustor modeling methods (see, e.g., Rosner[2]). It amounts to using this class of idealized spray combustors as an economical and unambiguous platform for evaluating the effects of important simplifying approximations—information that might otherwise be obscured, if not falsified, by additional modeling assumptions and numerical algorithms entering more "comprehensive" performance codes with vastly longer "turn-around times."

Instructive extensions (based on present/recent experience and/or anticipated future interest)

This bivariate population-balance study, along with its immediate univariate predecessor (Rosner et al.[1]), sets the stage for interesting and potentially important extensions—several of which have already been briefly mentioned above (tests of bivariate QMOM, and the distinct assumptions of "pseudo-unary" and intradroplet well-mixed behavior), already initiated. Beyond this, there are potentially instructive trivariate examples (e.g., EtOH + MeOH, or such ternarys as C_7H_{16} + $C_{12}H_{26}$ + methyl tertiary butyl ether, etc.). More complex fuel blends could be dealt with using the powerful formalism provided by "continuous mixture theory" when extended into the transport-domain (see, e.g., Arias-Zugasti and Rosner[14]).

For completeness, we should mention a rather different class of extensions, also be of interest—viz., the conceptual addition of a downstream adiabatic "plug-flow" reactor, which receives the output of our present "jet-stirred" primary reactor and enables an acceptably large fraction of the liquid fuel to ultimately vaporize and burn. Earlier theoretical studies of such 2-module representations of real combustors (see, e.g., Bragg,[22] Avery and Hart,[23] Rosner,[2] Rosner et al.[1]) demonstrated that such an "add-on" plug-flow-module in series would increase the overall combustor "efficiency" at the expense of overall combustor "intensity." Our present bivariate PBE-formulation and QS-droplet vaporization rate laws would enable such efficiency vs. intensity "tradeoffs" to be studied for important bio-fuels, perhaps for the first time.

Additionally, our discussion above about the disparity in the evaporation rates of EtOH ($+H_2O$) droplets compared with oxidizer droplets also suggests that it would be instructive to extend our present PB-methods to explicitly study bipropellant systems where both characteristic evaporation times are comparable—e.g., systems using the "storable" liquid oxidizer N_2O_4(L). In such cases, currently under investigation, there would be two droplet populations to consider simultaneously, both "coupled" via their shared vapor phase.

Concluding Remarks

As recently reviewed more thoroughly (Rosner[2]), the variety/complexity of spray combustors, together with the limited body of well-characterized/documented performance data in the public domain, continues to challenge design engineers. Yet, mathematical/numerical models, including the rather simple ones illustrated here, can provide valuable information about how device performance will depend on such factors as: combustor volume, inlet conditions, fuel properties, and injector performance. This information is potentially useful not only for engineering design but also to answer recently posed "what if" questions: e.g., the consequences of, say, fuel substitution, O_2 enrichment (in air-breathing systems), introduction of fuel blends or alcoholic extenders (e.g., butanol), etc. Accordingly, rational yet tractable computational models of this type can contribute to the shared goal of cutting the currently high cost of new spray combustor design and development.

In partial answer to the practitioner who may view the present class of models as "over-idealized," we believe that our recent studies reveal the extent to which population-balance methods and idealized chemical contactor concepts, central to a multiphase chemical reaction engineers "toolbox," can economically and relatively unambiguously demonstrate the value/consequences of proposed approximations. In this way, they can guide the economical development of more realistic, yet tractable, mathematical models of this class of rather complex devices. It will be especially

gratifying if these theoretical studies motivate creative new developments toward these shared goals.

Acknowledgments

The authors thank for the suggestions of Dr. M. Labowsky, the AIChE J reviewers of this manuscript, and support of the US National Science Foundation (via Yale grant #NSF/CTS 0522944), Ministerio de Ciencia e Innovación (via UNED grant #ENE2008-06515-C04-03), and Comunidad de Madrid (via UNED grants #S-0505/ENE/0229 and #S2009/ENE-1597).

Notation

$\mathcal{A}$ = Antoine equation parameter (Eq. 26, Table 2)
A = auxiliary function related to $\dot{\mu}$ (Eq. (30)
a = dimensionless droplet radius (R/R_{ref})
$\mathcal{B}$ = Antoine equation parameter (Eq. 26), Table 2)
B = auxiliary function related to $\dot{\omega}$ (Eq. 30)
B_{m} = mass-transfer driving force (see Eq. 4)
$\mathcal{C}$ = Antoine equation parameter (Eq. 26), Table 2)
c_{p} = specific heat at constant pressure
c = dimensionless specific heat at constant pressure ($c_{\mathrm{p}}/(L_{\mathrm{ref}}/T_{\mathrm{ref}})$)
D = Fick diffusion coefficient
Dam = (reference) Damköhler number ($t_{\mathrm{res}}/t_{\mathrm{vap}}$)
d_{32} = Sauter-mean diameter[16]
$F\ (Pe_{\mathrm{m}})$ = $[\ln\ (1 + B_{\mathrm{m}})]/B_{\mathrm{m}}$
k = Fourier thermal conductivity
L_{i} = latent heat of vaporization of species i
L_{ref} = reference scale of specific energy ($L_1\ (T_{\mathrm{b},1})$)
$\mathcal{L}_i$ = dimensionless vaporization latent heat (L_i/L_{ref})
m = total droplet mass ($m_1 + m_2$)
m_{ref} = characteristic mass ($\frac{4\pi}{3} R_{\mathrm{ref}}^3\ \rho_{\mathrm{ref}}^L$)
M = molecular weight (see Table 2)
n = number density distribution function of the steady-state spray in the chamber
n_{F} = NDDF of the "feed" spray
N = total number of droplets per unit volume in the combustion chamber
N_{F} = total number of droplets per unit volume in "feed" spray (corrected to chamber conditions)
p = constant chamber pressure
$p_{\mathrm{i}}^{\mathrm{sat}}$ = saturation pressure of species i
Pe_{m} = mass Peclet number (see Eq. 3)
R = droplet radius
R_{ref} = characteristic length ($d_{32}/2$)
$\mathcal{R}$ = universal gas constant
t = time
t_{res} = characteristic residence time ($\rho_{\mathrm{ch}}/\dot{m}_{\mathrm{V}}^{\mathrm{out}}$)
t_{ref} = reference time (t_{vap})
t_{vap} = characteristic QS vaporization time of a d_{32} droplet under reference conditions ($((1/3) \cdot (\rho_{\mathrm{ref}}^{\mathrm{L}}/\rho_{\mathrm{ref}}) \cdot (R_{\mathrm{ref}}^2/D_{\mathrm{ref}_0})$)
T = temperature
$T_{\mathrm{b},i}$ = boiling temperature of species i at current chamber pressure
T_{ref} = characteristic temperature ($T_{\mathrm{b},1}$)
T_{WB} = wet bulb temperature
x_i = mole fraction of species i
Z = $pV/(\mathcal{R}T)$

Greek letters

γ_i = activity coefficient of species i
$\delta(\ )$ = Dirac "delta" function
δ_i = $D_{i,\mathrm{f}}/D_{\mathrm{ref}}$
θ = dimensionless temperature (T/T_{ref})
λ = dimensionless thermal conductivity (k/k_{ref})
μ = dimensionless droplet mass
ρ = mass density
σ_{G} = geometric standard deviation
τ = dimensionless time (t/t_{ref})
Φ = effective chamber equivalence ratio ($(\mathrm{F/O})/(\mathrm{F/O})_{\mathrm{stoich}}$)
ω = droplet mass fraction of ethanol
ω_i = mass fraction of species i
ω_F = mass fraction of ethanol in "feed" spray

Subscripts and superscripts

0 = at initial time
1 = pertaining to species 1: ethanol
2 = pertaining to species 2: water
3 = pertaining to species 3: CO_2
4 = pertaining to species 4: oxygen
c = corresponding to the critical point
e = at exterior ("far" field for single droplet) gas conditions
F = pertaining to the fuel "feed" spray
f = at average "film" value in the gas (given by the 2/3 rule: $X_{\mathrm{f}} = (2/3)\ X_{\mathrm{w}} + (1/3)\ X_{\mathrm{e}}$)
L = pertaining to the liquid (spray) phase
ref = characteristic reference conditions
S = pertaining to the unvaporized fuel spray that leaves the chamber
vap = vaporization-based
V = pertaining to the vapor phase
w = at droplet surface

Abbreviations/acronyms

DSD = droplet size distribution
EOS = equation of state
EtOH = ethanol
MeOH = methanol
NDDF = number density distribution function
PBE = population balance equation
PDE = partial differential equation
QMOM = quadrature method of moments
QS = quasi-steady
stoich = corresponding to stoichiometric conditions
VLE = vapor–liquid equilibrium

Literature Cited

1. Rosner DE, Arias-Zugasti M, Labowsky M. Intensity and efficiency of spray fuel fed well-mixed adiabatic combustors. *Chem Eng Sci*. 2008;63:3909–3920.
2. Rosner DE. Spray combustor design/performance: chemical engineering contributions and the emergence of an "interacting population-balance" perspective. *Ind Eng Chem Res*. 2009;48:6453–6464.
3. Shyy W. *Computational Modeling for Fluid Flow and Interfacial Transport*. Mineola, NY: DOVER, 2006, 239–244; See Chapter VI, Section 1.
4. Rosner DE. *Transport Processes in Chemically Reacting Flow Systems*. Stoneham, MA: Butterworth-Heinemann, 1986; Reprinted 2000, Mineola, New York: DOVER (4th printing with 48p. appendix/updates).
5. Sutton GP. *History of Liquid Propellant Rocket Engines*. Reston, VA: AIAA, 2006.
6. Yaws CL. *Chemical Properties Handbook*. New York, NY: McGraw-Hill, 1999.
7. Sandler SI. *Chemical, Biochemical and Engineering Thermodynamics*, 4th ed New York, NY: Wiley, 2006.
8. Gaulhofer A, Kolbe B, Gmehling J. Thermodynamic properties of ethanol and water 3. Description of the different excess functions (G_E, H_E, $C_{p,E}$) using an empirical-model. *Fluid Phase Equilib*. 1988; 39:193–209.
9. Boyd JP. *Chebyshev and Fourier Spectral Methods*, 2nd ed. Mineola, New York: DOVER, 2000.
10. Rosner DE, Arias-Zugasti M. Condensation-induced surface boiling of alcohol fuel droplets in combustion chambers. *AIAA J Propul Power*. 2009;25:826–828.
11. Vemury S, Pratsinis SE. Self-preserving size distributions of agglomerates. *J Aerosol Sci*. 1995;26:175–185.
12. Rosner DE, Tassopoulos M. Deposition rates from polydispersed particle-populations of arbitrary spread. *AIChE J*. 1989;35:1497–1508.
13. Bensberg A, Roth P, Brink R, Lange H. Modeling of particle evolution in aerosol reactors with coflowing gaseous reactants. *AIChE J*. 1999;45:2097–2107.
14. Arias-Zugasti M, Rosner DE. Multicomponent fuel droplet vaporization and combustion using spectral theory for a continuous mixture. *Combust Flame*. 2003;135:271–284.

15. Rosner DE, Papadopoulos DH. Jump, slip, and creep boundary conditions at nonequilibrium gas/solid interfaces. *Ind Eng Chem Res*. 1996;35:3210–3222.
16. Davis EJ. A history and state-of-the art of accommodation coefficients. *Atmos Res*. 2006;82:561–578.
17. Lefebvre AH. *Atomization and Sprays*. Washington, DC: Taylor and Francis, 1989.
18. Lefebvre AH. *Gas Turbine Combustion*, 2nd ed. London, UK: Taylor and Francis, 1999.
19. Rosner DE, Arias-Zugasti M, LaMantia B. Calculation of Soret-shifted dew points by continuous mixture thermodynamics. *AIChE J*. 2005;51:2811–2824.
20. Landis RB, Mills AF. *Effect of internal diffusional resistance on the evaporation of binary droplets*. In *Proceedings of the Fifth International Heat Transfer Conference*. Tokyo: Japan Society of Mechanical Engineers, 1974;345–349.
21. Shaw BD, Aharon I, Lenhart D, Dietrich DL, Williams FA. Spacelab and drop-tower experiments on combustion of methanol/dodecanol and ethanol/dodecanol mixture droplets in reduced gravity. *Combust Sci and Technol*. 2001;167:29–56.
22. Bragg SL. *Application of Reaction Rate Theory to Combustion Chamber Analysis*, Report No. 16170 CF272. UK: Aeronautical Research Council, 1953.
23. Avery WH, Hart RW. Combustor performance with instantaneous mixing. *Ind Eng Chem*. 1953;45:1634–1637.

Manuscript received May 25, 2010, revision received Nov. 16, 2010, and final revision received Jan. 11, 2011.